Quaternary Research (2018), **90**, 222–243.
Copyright © University of Washington. Published by Cambridge University Press, 2018.
doi:10.1017/qua.2018.37

Global glacier dynamics during 100 ka Pleistocene glacial cycles

Philip D. Hughes[a]*, Philip L. Gibbard[b]

[a]Department of Geography, School of Environment, Education and Development, University of Manchester, Oxford Road, Manchester M13 9PL, United Kingdom
[b]Scott Polar Research Institute, University of Cambridge, Lensfield Road, Cambridge CB2 1ER, United Kingdom

(Received November 24, 2017; Accepted March 17, 2018)

Abstract

Ice volume during the last ten 100 ka glacial cycles was driven by solar radiation flux in the Northern Hemisphere. Early minima in solar radiation combined with critical levels of atmospheric CO_2 drove initial glacier expansion. Glacial cycles between Marine Isotope Stage (MIS) 24 and MIS 13, whilst at 100 ka periodicity, were irregular in amplitude, and the shift to the largest amplitude 100 ka glacial cycles occurred after MIS 16. Mountain glaciers in the mid-latitudes and Asia reached their maximum extents early in glacial cycles, then retreated as global climate became increasingly arid. In contrast, larger ice masses close to maritime moisture sources continued to build up and dominated global glacial maxima reflected in marine isotope and sea-level records. The effect of this pattern of glaciation on the state of the global atmosphere is evident in dust records from Antarctic ice cores, where pronounced double peaks in dust flux occur in all of the last eight glacial cycles. Glacier growth is strongly modulated by variations in solar radiation, especially in glacial inceptions. This external control accounts for ~50–60% of ice volume change through glacial cycles. Internal global glacier–climate dynamics account for the rest of the change, which is controlled by the geographic distributions of glaciers.

Keywords: Glaciation; orbital forcing; glacial cycles; ice sheets; glaciers; Pleistocene

INTRODUCTION

The Quaternary is often subdivided on the basis of fluctuations in climate changes, most recently using the marine oxygen isotope record (Fig. 1), and has been for decades, starting in the 1950s (Arrhenius, 1952), with numerous developments since (cf. review in Railsback et al., 2015). This is a record of global ice volume and provides the main basis for defining glacial cycles (Lisiecki and Raymo, 2005). However, it is important to appreciate that this approach is essentially climatostratigraphy and not chronostratigraphy (Gibbard and West, 2000; Gibbard, 2013), although the Quaternary has been subdivided and defined in chronostratigraphic terms (e.g., Martinson et al., 1987). The marine isotope record is clearly a valuable global reference for subdividing the Quaternary, and the scheme of stages and substages in the marine isotope record continues to underpin the Quaternary time scale (Lisiecki and Raymo, 2005; Railsback et al., 2015) (Fig. 1). Whilst this paper focuses on the Quaternary glacial cycles, the general principles are also applicable to earlier glacial cycles, such as the mid-Oligocene glacial maximum and the late Pliocene M2 glaciation (3.3 Ma), both of which are also defined with reference to the marine isotope record (Harzhauser et al., 2016; De Schepper et al., 2014).

In contrast to the quasi-continuous sedimentary sequences on the deep-ocean floors, the glacier records on land are inherently fragmentary. At the surface, morphostratigraphic preservation of glaciations is directly related to the diminishing size of successive glaciations. In other words, if the most recent glaciation is the largest in extent, then evidence for earlier glaciations will be removed, or at least remoulded or reworked. However, this is not always the case, and it is possible for previous glaciations to be preserved beneath deposits of later glacier advances or in landscape depressions, especially in lowland environments. Nevertheless, even in these situations the glacier record is prone to fragmentation. Despite these challenges, there is direct evidence for glaciations throughout the Quaternary and before (Ehlers and Gibbard, 2007, 2008), although clearly the best potential for dating and understanding the spatial and climatic significance of past glaciers originates from the more recent late and middle Pleistocene glaciations. Ehlers et al. (2011a) found that the succession of glaciations reported from four of the last 10 glacial cycles (Marine Isotope Stage [MIS] 16, 12, 6, and 5d–2) is striking in that it is repeatedly found in many

* Corresponding author at: Department of Geography, School of Environment, Education and Development, University of Manchester, Oxford Road, Manchester M13 9PL, UK. E-mail address: philip.hughes@manchester.ac.uk (P. D. Hughes).

https://doi.org/10.1017/qua.2018.37 Published online by Cambridge University Press

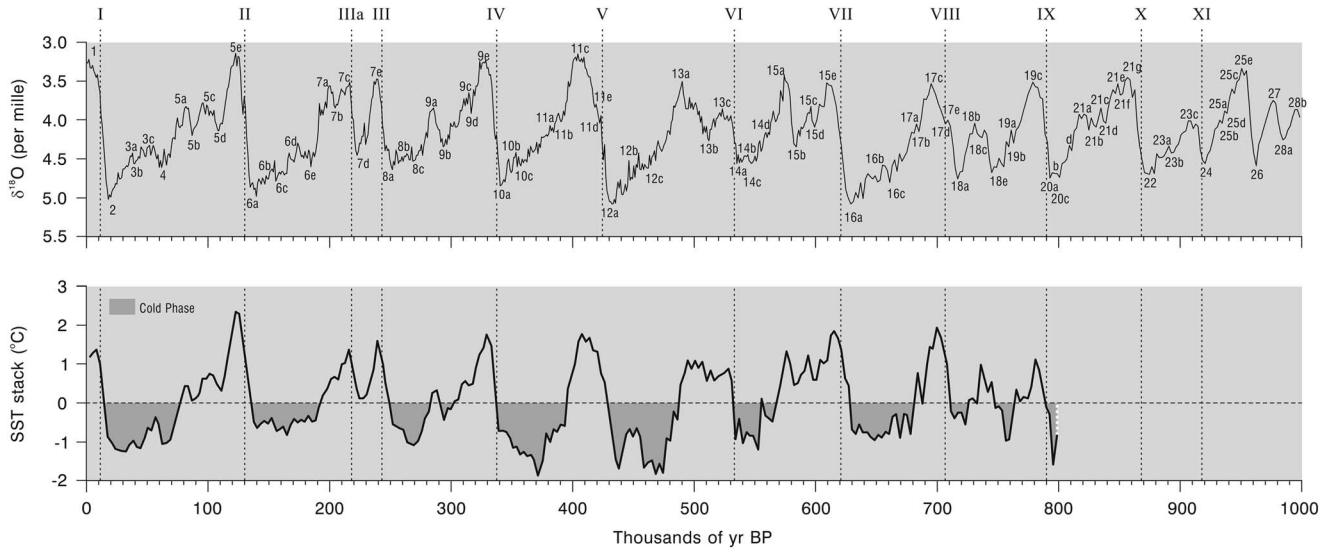


Figure 1. Marine oxygen isotope stratigraphy from the Lisiecki and Raymo (2005) global stack of 57 sediment cores. The stages are from Lisiecki and Raymo (2005), and the substages beyond MIS 5e are from Railsback et al. (2015).Terminations are indicated, and the ages of these are from Raymo (1997), Lisiecki and Raymo (2005), and Cheng et al. (2009). The lower graph shows global sea-surface temperature (SST) data from Shakun et al. (2015), which are derived from a stack of 49 paired planktonic δ^{18}Op-SST records from the global oceans.

areas of the world, and the absence of records of glaciations during other glacial cycles reflects the fact that these glaciations were less extensive. Even for the late Pleistocene, the glacier records are fragmentary and hindered by the fact that successively diminishing glacier extents are recorded at the land surface. This has been compounded, until recently, by the difficulty in numerically dating glacial sequences. Recent advances in geochronology, especially cosmogenic exposure dating and new luminescence techniques, have now revealed a complex spatial and temporal pattern of glaciation, with many areas seeing maximum glacier advances early in the last glacial cycle, but others seeing maximum advances at or close to the global last glacial maximum (LGM; Hughes et al., 2013).

It is now clear from the last glacial cycle that glacier advances were driven by a complex interplay of air temperatures and precipitation patterns. Glacier advances are controlled by the balance between accumulation and ablation, which is largely, though not entirely, driven by precipitation in the form of snow and summer air temperatures, respectively (Ohmura et al., 1992; Hughes and Braithwaite, 2008). This means that glaciers advance depending on the combination of *both* accumulation and ablation. For example, many glaciers in the mid-latitudes and in the continental interiors did not advance through MIS 2 (= Late Weichselian/Wisconsinan, etc.) and the global LGM but instead suffered retreat. This was because increasing aridity, which occurred as the large continental ice sheets reached their peak size, offset the increasingly colder air temperatures. In some areas glaciers advanced in warmer intervals of the last glacial cycle, such as MIS 3 (= Middle Weichselian/Wisconsinan, etc.), when moisture supply (and therefore winter precipitation) was greater (Hughes et al., 2006), whereas in other areas glaciers reached their maximum extent in the major cold and globally dry intervals, such as MIS 4 (= Early Weichselian/Wisconsinan, etc.). Thus, the pattern of global glaciations is not simply reflected by concepts as the LGM. The characteristics of the last glacial cycle were very likely to be the same during earlier glacial cycles (Head and Gibbard, 2015).

The structure of glacial cycles and changes in their pattern through time has been examined by many authors, including Imbrie et al. (1993), Paillard (2001), and Lang and Wolff (2011). However, discussions of glaciation are usually focused on dynamics of the largest continental ice sheets. In this paper, the focus is on the nature of global glaciation during these glacial cycles and the role glaciers in different parts of the world play in driving and defining global climatic cycles. Apart from a general appreciation of the size and distribution of ice during maximum glacier advances throughout earlier glacial cycles, such as MIS 6, 12, and 16, very little attention has been paid to the spatial and temporal patterns and climatic significance of glaciations that are recorded within these and other glacial cycles.

This paper examines the extent and timing of glaciations during the last 10 glacial cycles between MIS 1 and MIS 25 (the last ~925 ka). This interval is chosen because MIS 22–24 (= Bavelian Stage), was the first of the major *global* glaciations with substantial ice volumes in both hemispheres that typify the later Pleistocene glaciations (Ehlers and Gibbard, 2007). The focus is on the pattern of glaciation through glacial cycles recorded in glacier records themselves and also indirectly using evidence from in the polar ice cores and the benthic marine oxygen isotope records. These records of glaciation are then compared with drivers of climate, such as insolation and

https://doi.org/10.1017/qua.2018.37 Published online by Cambridge University Press

atmospheric CO_2. The aim of this research is to: (1) examine evidence of global patterns of glacier behaviour during multiple glacial cycles and (2) examine how these patterns of glaciation can be explained by variations in solar radiation, atmospheric CO_2, global sea-surface temperatures (SSTs), and other driving factors, including glaciers themselves.

METHODOLOGY AND APPROACH

The data include the direct evidence of glaciation in the geological and geomorphological record, coupled with analysis of the structure of glacial cycles recorded in ice cores and marine sediments. Patterns of glaciation and climate change indicated in these records are then compared to solar variations through glacial cycles. The results are then used to inform discussion on the problems and prospects for the fine-scale stratigraphic division of cold stages. The term "cold stage" refers to climatostratigraphic/chronostratigraphic units such as the Weichselian or Wisconsinan in Europe or North America, respectively. Climatic subdivisions have been used interchangeably with chronostratigraphic stages by the majority of workers (Gibbard, 2013). The last cold stage (Weichselian, Wisconsinan, or equivalents) is correlative to MIS 5d–2 in the ocean-floor marine isotope stratigraphy. For some earlier glacial intervals, terrestrial chronostratigraphic units may not always be formally defined, and there are pitfalls associated with direct terrestrial–marine correlation (Gibbard and West, 2000). Nevertheless, in recent years it has become common practice to directly correlate terrestrial sequences with those in the oceans (Gibbard, 2013). A global chronostratigraphic table for the whole Quaternary is provided in Cohen and Gibbard (2011) and also in the Subcommission on Quaternary Stratigraphy (2017).

Glacier records

Evidence of glaciation in the geological and geomorphological records is well documented. Reviews of global glaciations have been published in the edited volumes of Denton and Hughes (1981), Ehlers et al. (2011b), and Ehlers and Gibbard (2004) and also in review papers by Ehlers and Gibbard (2007, 2008). The last cold stage (MIS 5d–2; Weichselian, Wisconsinan) is the best studied owing to the often excellent preservation and strong geochronological control. A review of global glaciations during the last cold stage is provided in Hughes et al. (2013).

Ice-core data

Ice-core records provide information on the state of the atmosphere through time. The Greenland ice-core records span the last glacial cycle, whilst the Antarctic ice-core records span the last eight glacial cycles. The former have been used extensively to provide an event stratigraphy for the last glacial cycle (Lowe et al., 2008; Blockley et al., 2012; Hughes and Gibbard, 2015). For earlier glacial cycles we must rely on the records from Antarctica. The deuterium-derived temperature plot from Antarctica provides a record of global climate fluctuations (European Project for Ice Coring in Antarctica [EPICA], 2006). However, ice-core records of climate from Greenland and Antarctica show asynchronous temperature variations on millennial time scales during the last cold stage (Blunier et al., 1998; EPICA, 2006; Jouzel et al., 2007a; Stenni et al., 2011). Dust concentrations in polar ice cores can provide insight into the state of the atmosphere through time. In Antarctica, dust recorded in ice cores is derived from South America during glacial periods and Australia during interglacial periods (Lambert et al., 2012). Dust flux over Antarctica has a close correlation with temperature as climate becomes colder (Lambert et al., 2008). This means that during glacial periods, dust acts as a proxy for temperatures over Antarctica. Whilst dust in Antarctic ice cores has a southern hemispheric source, the dramatic increase in dust flux in glaciations (×25) is enabled by a globally reduced hydrological cycle (Lambert et al., 2008). Comparison of Antarctic ice-core dust records with the magnetic susceptibility record of loess/palaeosol sequences from the Chinese Loess Plateau (Kukla et al., 1994) confirms the synchronicity of global changes in atmospheric dust load (Lambert et al., 2008). In addition to temperature and dust records, ice-core data were utilised for analysing CO_2 through glacial cycles. Ganopolski et al. (2016) showed that CO_2 in conjunction with solar radiation input to high northern latitudes is an important control on glacial inception.

Marine isotope data

The marine oxygen isotope record currently provides the main basis for defining and subdividing the full span of the Quaternary at the global scale (e.g., Imbrie et al., 1984; Martinson et al., 1987; Lisiecki and Raymo, 2005; Railsback et al., 2015). Marine oxygen isotopes have been established as a proxy for global ice volume since the 1960s (e.g., Shackleton, 1967), although the isotopic record is also known to be affected by deep-water ocean temperature (Shackleton, 2000). Orbital forcing has long been identified as the driver of cyclic fluctuations in marine oxygen isotopes (Hays et al., 1976), and the frequency of orbital variations has underpinned the time frame to which the marine isotope record is tuned (Imbrie et al., 1984, Ruddiman et al., 1989; Lisiecki and Raymo, 2005). The LR04 benthic stack is based on 57 globally distributed benthic $\delta^{18}O$ records. (Lisiecki and Raymo, 2005) and is a record of both global ice volume and deep-ocean temperature. For assessing the severity of glacial cycles in terms of ice volume using marine isotope data, both the maximum and the top 5% percentile $\delta^{18}O$ values from the Lisiecki and Raymo (2005) stack were considered (Table 1). The latter is likely to be more representative, since $\delta^{18}O$ values in the Lisiecki and Raymo (2005) stack are an orbitally tuned average of 57 cores, with leads and lags of up to 5 ka known (up to 5% of 100 ka cycles) between oxygen isotope records from different ocean basins (Skinner and Shackleton, 2005). These

https://doi.org/10.1017/qua.2018.37 Published online by Cambridge University Press

Table 1. The definitions of the last 10 full glacial cycles based on the marine isotope stratigraphy: (1) the boundaries of the glacial cycles are defined by termination ages provided in Raymo (1997), Lisiecki and Raymo (2005), and Cheng et al. (2009); (2) cold "phases" are defined as periods when the global sea-surface temperatures (derived from global marine oxygen isotope records) were ≤0°C (Shakun et al., 2015); (3) the numbering and span of the cold stages/substage intervals are based on Lisiecki and Raymo (2005) and Railsback et al. (2015). Detrended global sea-level values were obtained from Shakun et al. (2015). Percentiles (top 5% for $\delta^{18}O$ and bottom 25% for sea levels) are based on the glacial marine isotope stage/substage subdivisions (definition 3 in this table).

Glacial cycles: definition in the marine isotope records			1. Length of glacial cycle (termination to termination)	2. Cold "phase" length	3. Length of "cold stage" marine isotope stage/ substage subdivisions	Maximum $\delta^{18}O$ value (per mille and corresponding age)	Top 5% $\delta^{18}O$ (per mille)	Detrended global sea level (m) – lower quartile
Basal termination and age	Preceding interglacial stage/substage	"Cold stage" marine isotope stages						
I [11.7 ka[a]]								
II [130 ka]	5e	5d–2	118 ka	57 ka	103 ka	5.02 [18 ka]	4.88	–83
IIIa [225 ka]	7a	6	95 ka	54 ka	61 ka	4.98 [140 ka]	4.83	–115
III [243 ka]	9e	8	94 ka	51 ka	77 ka	4.63 [252 ka]	4.53	–78
IV [337 ka]	11c	10	87 ka	54 ka	37 ka	4.84 [341 ka]	4.79	–94
V [424 ka]	13a	12	109 ka	57 ka	58 ka	5.08 [433/434 ka]	5.06	–109
VI [533 ka]	15a	14	88 ka	33 ka	30 ka	4.55 [548 ka]	4.55	–46
VII [621 ka]	17c	16	85 ka	51 ka	69 ka	5.08 [630 ka]	5.02	–100
VIII [706 ka]	19c	18	84 ka	21 ka	60 ka	4.75 [718 ka]	4.66	–85
IX [790 ka]	21g	20	76 ka	15 ka	55 ka	4.73 [802 ka]	4.70	
X [868 ka]	25e	24–22	95 ka	Limited data	93 ka	4.69 [876 ka]	4.68	
XII [963 ka]								

[a]From Walker et al., 2009.

leads and lags are associated with deep-ocean circulation and variations in ocean temperatures that also affect the marine oxygen isotope record (Labeyrie et al., 1987; Shackleton, 2000; Waelbroeck et al., 2002; Elderfield et al., 2012).

Shakun et al. (2015) exploited the temperature component of the oxygen isotope record to extract SSTs from planktonic $\delta^{18}O$ records from 49 cores around the globe. This enables insights into global shifts in both climate and ice volume during glacial cycles: one using the benthic stack of Lisiecki and Raymo (2005) and the other using the global SST stack of Shakun et al. (2015). Whilst it is possible to extract and model arbitrary measures of ice volume from $\delta^{18}O$ data (fig. 7d in Shakun et al., 2015), this requires assumptions on orbital forcing when it is known that other internal climate forcings are at play, such as land–ocean interactions including glacier distributions in themselves (this paper) and global SSTs (Shakun et al., 2015, p. 66). However, Shakun et al. (2015) were able provide a first attempt to correct the $\delta^{18}O$ stack for non–ice volume effects, thus enabling the $\delta^{18}O$ stack to be used as a direct proxy for global ice volume. Whilst these detrended sea-level data represent an indirect proxy, they are used here as the best estimate of shifts in global ice volume.

In addition, using the global SST data presented in Shakun et al. (2015), it is possible to identify sustained global cold "phases" within glacial cycles in addition to the ice volume signal. Sustained cold phases are defined here as intervals when global SST is ≤0°C for at least *20 ka*, with interruptions of no more than *10 ka* (see Fig. 1, bottom graph; SST curve from Shakun et al., 2015).

Solar radiation

Solar radiation variations at 60°N were used as a proxy for summer ablation potential at both high and mid-latitudes. Apart from Antarctica, the Southern Hemisphere is not significant for glacier build-up in the mid-latitudes at a global scale, because the land masses are very small in comparison with the Northern Hemisphere. Solar radiation data are derived from Berger and Loutre (1991) and Berger (1992).

GLACIAL CYCLES: DEFINITIONS AND SUBDIVISION

Glacial cycles are major climatic oscillations that can be defined using the marine isotope record and their shape and frequency can be determined using various criteria (e.g., Fairbridge, 1972; Raymo, 2007). However, the definition of the span of glacial cycles was discussed by Fairbridge (1972, p. 286), who noted that "there is no logical mathematical solution, and the International Stratigraphic Commission rightly ignores any such theoretical proposals." This remains the case today, and the concept of the glacial cycle defined in the marine isotope record has no stratigraphic basis; instead, cold periods within glacial cycles are defined by chronostratigraphic cold stages such as the Weichselian or Wisconsinan for the last glacial cycle in Europe and North America, respectively. Nevertheless, the marine isotope record is a useful tool for assessing global climatic shifts, and glacial cycles can be defined as the interval between glacial terminations encompassing both the preceding interglacial period

https://doi.org/10.1017/qua.2018.37 Published online by Cambridge University Press

and the following cold stages (Broecker and van Donk, 1970; Fairbridge, 1972). The ages of the last seven major terminations are listed in Raymo (1997) and Lisiecki and Raymo (2005, their table 3), with an additional age for termination IIIa defined in Cheng et al. (2009). The ages of terminations before termination VII can be obtained from Railsback et al. (2015, their fig. 3 and references therein). Following this approach, the last glacial cycle is defined as the period between termination II and termination I encompassing both the last interglacial period (= Eemian Stage and equivalents) and also the last cold stage (= Weichselian Stage and equivalents).

Three approaches were used for describing glacial cycles:

1. the periods between glacial terminations (this defines the glacial cycle);
2. the periods of cold phases defined by global SSTs within glacial cycles (cf. Shakun et al., 2015); and
3. the span of traditional subdivision of cold stages based on marine isotope stages and substages (Railsback et al., 2015).

Termination positions and global SSTs are shown in Figure 1 with reference to the marine isotope stages and substages (cf. Railsback et al., 2015; Shakun et al., 2015). The use of terminations to define the boundaries of glacial cycles works effectively for most glacial periods. Terminations have been associated with ice sheet instability and collapse at the end of glacial cycles (MacAyeal, 1993), thus indicating a glacier-forcing mechanism for limiting the length of glacial cycles. However, other factors have also been suggested, including increases in greenhouse gases such as CH_4 and CO_2 (Capron et al., 2016), although determining cause and effect is difficult given the interrelationships involved. Whatever their cause, there is no disputing the importance of terminations in controlling global ice volume, and thus they represent an apt marker for defining many, though not all, glacial cycles. The only exception is for MIS 24–22, and this stems from debate regarding MIS 23 and its classification as an interstadial or interglacial period (see "MIS 23–22 (termination XI to X) or 25–22 (termination XII to X)").

PATTERNS OF GLACIATION DURING GLACIAL CYCLES

When defined from termination to termination, glacial cycles varied considerably in duration during the past million years. The two longest glacial cycles by this definition encompassed the glacial intervals of MIS 5d–2 and MIS 12 (118 and 109 ka, respectively). All other glacial cycles were bounded by terminations 76 to 95 ka apart. Significantly, the last full five glacial cycles were all longer than the preceding five. Cold phases within the last five glacial cycles were remarkably similar in length (51–57 ka; mean = 54.6 ± 2.6 ka SD) (Table 1). However, the glacial cycles incorporating MIS 14, 16, 18, and 20 were largely characterised by short cold phase lengths (33, 51, 21, and 15 ka) (there are no global SST data for MIS 22–24 in Shakun et al., 2015). Only MIS 16 had a cold phase length similar to the last five cycles. The cold stages with the greatest maximum $\delta^{18}O$ value of all of the last 10 glacial cycles (and the entire Quaternary) were MIS 16 and 12 (both 5.08 per mille), followed by MIS 5d–2 (5.02 per mille). The cold stage with the lowest maximum $\delta^{18}O$ value was MIS 14 (4.55 per mille). However, when global SSTs are decoupled from the marine isotope record, then the most severe glacial intervals are MIS 12 and 10, whereas MIS 14 and 16 appear to have been of similar severity (Fig. 1). The final approach for describing glacial cycles, using marine isotope stage and substage lengths, provides another perspective. This approach identifies MIS 5d–2 as the longest interval (103 ka), whereas MIS 12 is almost half this length (58 ka) despite the latter being defined as a long glacial cycle when defined using terminations. These contradictions are not simply the artefacts of stage/termination boundary definitions but must also have some physical basis. For example, stage/substage boundaries closely correspond with glacial inceptions defined using solar/CO_2 models (Ganopolski et al., 2016), whilst terminations have a clear physical basis in ice-sheet dynamics. The contradictions apparent in the various definitions of glacial cycles stem from the complexity of the global climate signal that is recorded in different environmental systems.

Understanding the record of changes to the global cryosphere requires a closer look at the evidence for glaciation and associated proxy evidence during the different glacial cycles. This is done in the following sections for each of the last 10 glacial cycles. In this analysis we use marine isotope stratigraphy to identify time intervals within glacial cycles in conjunction with continental European chronostratigraphic terminology (and other terminologies) to describe terrestrially defined cold stages.

MIS 5e–2 (terminations II to I)

The span of the last cold glacial cycle (termination II to I) is the longest of all the glacial cycles at 118 ka. The end of the last interglacial period (MIS 5e) is placed at ca. 115 ka in the marine isotope record, based on a substantial cooling effect at this time (Shackleton et al., 2002, 2003).

The last cold stage (Weichselian Stage) has two distinct and pronounced cold episodes during MIS 4 and 2. The paired cold-stage phenomenon of MIS 4 and 2 is also highlighted in dust and temperature records from Antarctica (Fig. 2). The dust flux peaks in the Antarctic ice cores for MIS 4 and 2 are 13.7 and 18.2 $mg/m^2/a$, respectively. The estimated temperature difference over Antarctica (compared to the average of the past 1 ka) reached minima of −10.2°C and −10.6°C, for MIS 4 and 2, respectively (Fig. 2).

MIS 4 and 2 are separated by the warm interval of MIS 3, which is not considered a true interglacial period, but an interstadial complex with climate oscillating on a 100–1000 yr time scale between near-interglacial and peak-glacial conditions (van Andel, 2002). This high-amplitude millennial-scale climatic instability is evident in both Greenland and Antarctic ice-core records (Blunier et al., 1998; Markle et al., 2017).

https://doi.org/10.1017/qua.2018.37 Published online by Cambridge University Press

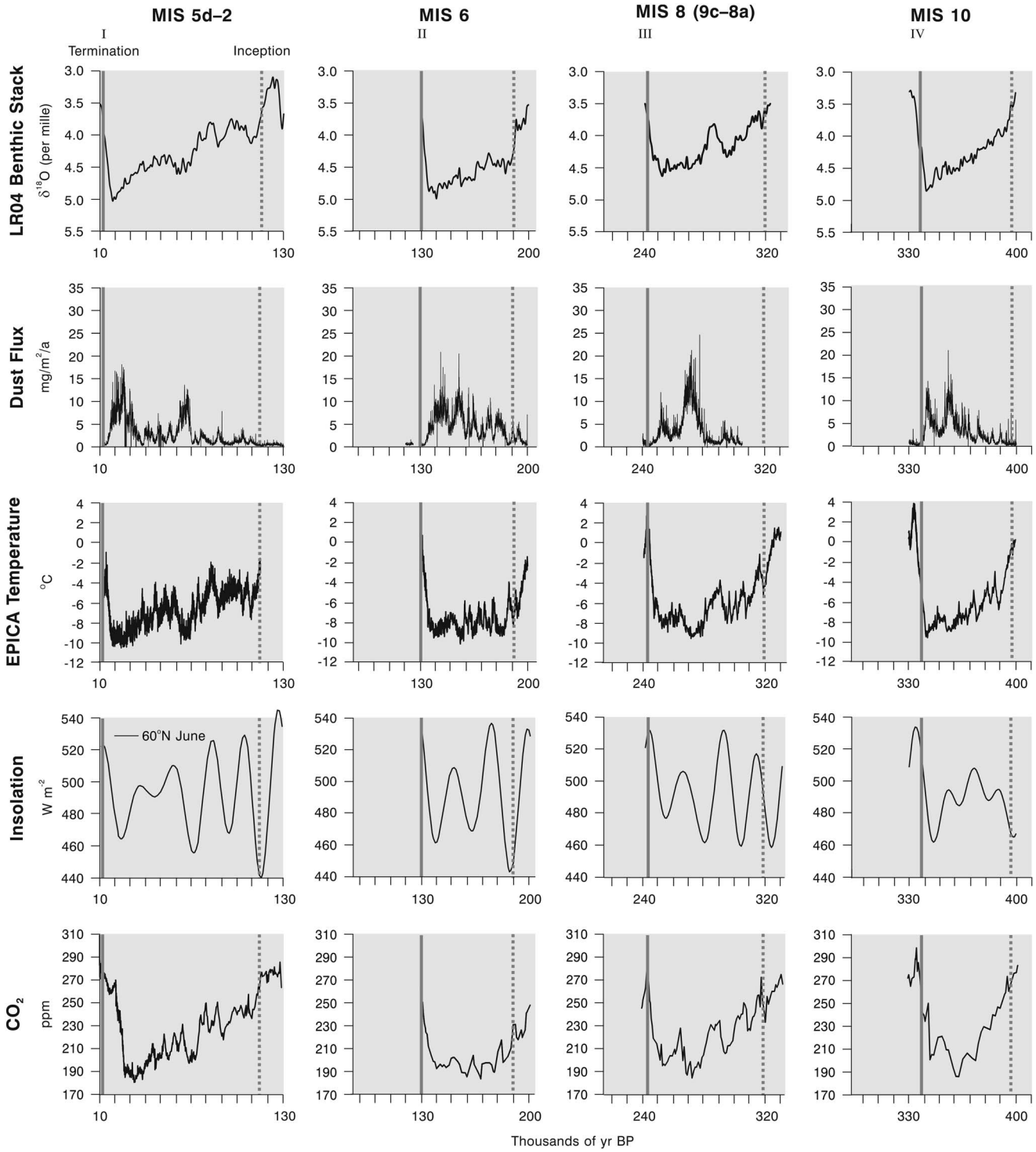


Figure 2. The last 8 glacial cycles (MIS 5d–2 to MIS 18) showing data over these periods from (i) the benthic $\delta^{18}O$ stack of Lisiecki and Raymo (2005), (ii) dust flux from the EPICA Dome C ice-core record (Lambert et al., 2012), and (iii) temperature curves derived from the EPICA Dome C ice-core deuterium record (Jouzel et al., 2007b, 2007c). The temperature estimate in this curve is the estimated temperature difference over Antarctica compared with the average of the past 1 ka, (iv) insolation at 60°N from Berger and Loutre (1991) and Berger (1992), (v) CO_2 data are from the Antarctic ice cores revised 800 ka CO_2 data (Bereiter et al., 2015; National Oceanic and Atmospheric Administration, 2018).

The terrestrial glacial record for the last glacial cycle is reviewed in detail in Hughes et al. (2013), who noted the asynchronous record of glaciation around the world. In particular, many glaciers advanced early in the glacial cycle, especially in Asia (Svendsen et al., 2004; Larsen et al., 2006; Vorren et al., 2011; Astakhov, 2018) and mid-latitude mountains, with the latter phenomenon highlighted in a seminal paper by Gillespie and Molnar (1995). Even in

https://doi.org/10.1017/qua.2018.37 Published online by Cambridge University Press

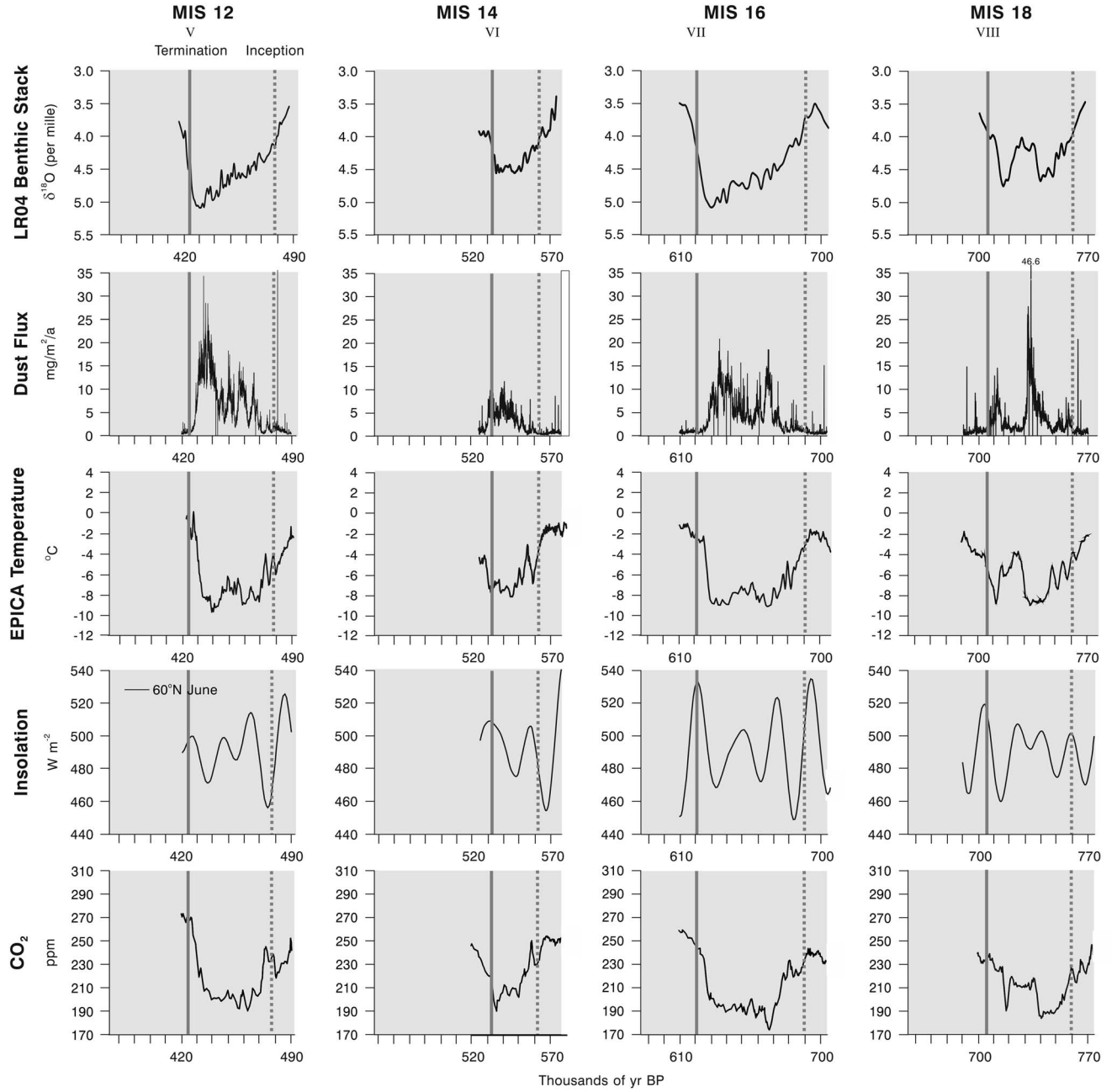


Figure 2. Continued.

Antarctica, there is evidence that the ice sheets were thicker before the global LGM, and the ice in the centre of the East Antarctic Ice Sheet was no thicker at the LGM than it is today (Lilly et al., 2010). Also, in the southern parts of the McMurdo Dry Valleys area of the Transantarctic Mountains, terminal moraines associated with the local LGM with a mean age of 36 ± 8 ka are at most only 100 m from the current ice margin (Joy et al., 2017).

MIS 7–6 (terminations III to II)

Some marine $\delta^{18}O$ records suggest that global ice volume was greater in MIS 6 (Saalian Stage) than in MIS 2 (Shackleton, 1987; Roucoux et al., 2011). This is supported by the lower quartile value of global sea levels indicated in the data calculated by Shakun et al. (2015). However, in the Lisiecki and Raymo (2005) stack of 57 records, MIS 2 has a slightly higher $\delta^{18}O$ than MIS 6, although the ice volume signal may be masked by temperature effects, since global SSTs were warmer in MIS 6 than during MIS 5d–2 (Fig. 1). Warmer global SSTs during MIS 6 may have allowed greater moisture supply to drive some ice masses to larger extents than in other colder glacial periods. Also, the distributions of global ice were different at the penultimate glacial maximum (PGM) compared with the LGM, with much larger ice masses over Eurasia in the PGM compared with the LGM, and smaller ice masses over North America at the PGM compared

https://doi.org/10.1017/qua.2018.37 Published online by Cambridge University Press

with the LGM (Rohling et al., 2017). The peak of the PGM occurred at ca. 140 ka (Stirling et al., 1998; Railsback et al., 2014; Colleoni et al., 2016).

The amplitude of precessional-scale solar variability at 60°N was large for MIS 6, larger than for MIS 5d–2, and many of the last 10 glacial cycles (Fig. 2). This resulted in major peaks in summer insolation in the middle of the glacial cycle. The middle of MIS 6 (MIS 6e, 166–178 ka) is characterised by a humid period in speleothem records from Israel (Ayalon et al., 2002), southern Tuscany (Bard et al., 2002), and the Apuan Alps (Regattieri et al., 2014). However, despite corresponding to a major peak in insolation, this interval was also relatively cool in Europe and the Mediterranean region, with few temperate trees compared to the analogous situation of MIS 3 in the last glacial cycle (Roucoux et al., 2011). Climate in this interval does exhibit large-amplitude millennial-scale variability like MIS 3, but unlike the last glacial cycle, there is no evidence of major ice rafting, nor Heinrich events, from MIS 6 (McManus et al., 1999; Margari et al., 2010). This suggests a different configuration of ice around the North Atlantic compared with the last glacial cycle.

The lack of trees in mid-latitude Europe during MIS 6e, compared to the analogous situation in MIS 3, is also matched by the most prolonged savannah phase of the last 540 ka at Lake Botsumtwi in Ghana, West Africa. The global dust signal recorded in the Antarctic ice cores is also more sustained through MIS 6 than during MIS 5d–2, with a pronounced dust peak in MIS 6e (Fig. 2). This hints at a significant global hydrological perturbation in this interval associated with a major build-up of ice volume, although the evidence of humidity in the Mediterranean region at this time highlights the complex response of the climate system to such events.

The glacial maximum of MIS 6 was the most extensive glaciation of the last 400 ka over Eurasia, the biggest since MIS 12 (Colleoni et al., 2016). In Europe, MIS 6 is recorded by the largest ice advance of the Saalian Stage, during the Drenthe Stadial. This was several hundred kilometres beyond the later Weichselian Stage (MIS 5d–2) limits in the Netherlands and northern Germany (Ehlers et al., 2011c; Laban and van der Meer, 2011) and more than 100 km beyond in eastern Germany and Poland (Ehlers et al., 2011c; Marks, 2011). The ice also extended further southeast and east than the Weichselian Stage ice sheet in Russia and neighbouring states (Astakhov, 2004); overall it was 56% larger in volume. The maximum glacier limits of the Saalian Stage in northern Europe were also more extensive than the earlier Elsterian Stage glaciation (MIS 12), and thus the Saalian Stage constitutes the most extensive glaciation recorded in a large part of northern continental Europe.

Compared to the LGM, the maximum extent of the MIS 6 glaciation in Eurasia was characterised by an overall considerably more extensive ice sheet. During the late Saalian Drenthe Stadial (early MIS 6) in Europe, the Fennoscandian Ice Sheet reached its maximum extent in the central Netherlands, Germany, Britain, and the Russian Plain. This was followed by ice-sheet melting under increasing summer insolation and sea-level rise at ca. 157 ka, the most extreme conditions occurring at ca. 157–154 ka (Margari et al., 2010; 2014). After ca. 150 ka, eustatic sea-level records and glacial geological evidence suggest that ice sheets readvanced, with global ice volume reaching its maximum extent towards the end of MIS 6, reflecting the maximum growth of the Illinoian ice sheet in North America (e.g., Curry et al., 2011; Syverson and Colgan, 2011). In Europe, the Warthe Stadial I and II ice advances were markedly less extensive than during the previous Drenthe (Ehlers et al., 2011c), but that may have been compensated for by ice expansion in Russia and Siberia (e.g., Astakhov, 2004; Astakhov et al., 2016).

In England the Saalian Stage-equivalent, the Wolstonian Stage glaciation, is represented by a large ice lobe that reached the Fenland basin in eastern England, and Midland England. This has again been correlated with MIS 6 (Gibbard et al., 2011; 2018) and represents the second-largest recorded glaciation in eastern Britain, smaller than the earlier Anglian Stage glaciation (MIS 12) and larger than the later Devensian Stage glaciation (MIS 5d–2).

The largest ice masses of Eurasia in the equivalent of the Saalian Stage were present over Russia. However, unlike in Europe, the MIS 6 glaciation equivalent in Siberia was less extensive than during the earlier MIS 8 (Samarovo glaciation) —see below [MIS 9–8 (termination IV to III)] and Fig. 3.

In North America the Illinoian glaciation is equivalent to MIS 6. Here, the southern margin of the Laurentide Ice Sheet extended 150 km beyond the later Wisconsinan (MIS 5d–2) limits in Illinois (Curry et al., 2011) at a peak of 140 ka (Colleoni et al., 2016). In Wisconsin the Illinoian Stage glacial limits were only a maximum of 30 km beyond Wisconsinan limits, and in some places the latter was more extensive (Syverson and Colgan, 2011).

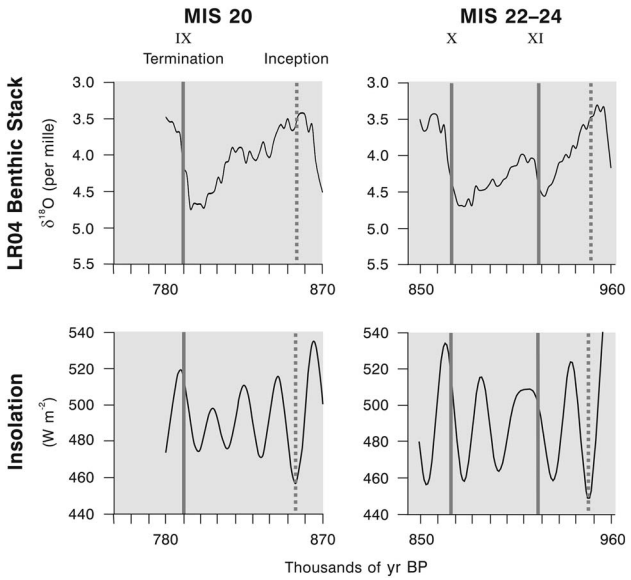


Figure 3. Benthic marine δ18O isotope record (from Lisiecki and Raymo, 2005) and solar radiation at 60°N and 30°N [full and dashed lines, respectively; from Berger and Loutre (1991) and Berger (1992)] for MIS 20 and 22–24. These intervals are beyond the ice-core data records used in Fig. 2 and are therefore shown separately.

https://doi.org/10.1017/qua.2018.37 Published online by Cambridge University Press

In the high mountains of central Asia, the penultimate glaciation (MIS 6) was more extensive than the last cold stage in several areas (Owen and Dortch, 2014). This has been revealed by ^{10}Be exposure age dating from the Pamirs (Seong et al., 2009; Owen et al., 2012) and the Karakoram (Seong et al., 2007).

MIS 9–8 (terminations IV to III)

This cold stage incorporates MIS 9c to MIS 8a. The structure of this glacial cycle is marked by a strong interstadial (MIS 9a) separating two glacial troughs (MIS 8a–c and 9b). MIS 8a represents the most severe part of the glacial cycle in terms of ice volume and lowest global sea levels (Lisiecki and Raymo, 2005; Shakun et al., 2015). Overall, this was a relatively weak glacial cycle, second only to MIS 14 in terms of maximum δ^{18}O values for the last 10 glacial cycles and the weakest in terms of the uppermost 5% percentile (Table 1).

As with MIS 10 (discussed in the following section), the dust peak in Antarctica does not coincide with the glacial maximum of MIS 8 recorded in the marine isotope curve. Instead, it occurs earlier, at ca. 272 ka, with a smaller peak at 252 ka coinciding with the isotopic glacial maximum. The first dust peak also coincides with the lowest CO_2 levels and the coldest global SSTs of this glacial period (Figs. 2 and 1, respectively). A very large, isolated, single-layer dust peak at 277 ka may be related to an extraterrestrial impact event, as has been shown for MIS 12 (Misawa et al., 2010), although further research is needed to prove this.

The nature of environmental changes on land during this glacial cycle has been revealed by high-resolution pollen analysis from Tenaghi Philippon in Greece (Fletcher et al., 2013). Forest expansion events occurred during the early glacial period (equivalent to MIS 9c–a) and during mid- to late MIS 8, but are absent from the early part of MIS 8. This lack of trees in Greece early in MIS 8 corresponds with the largest dust peak in Antarctica at ca. 272 ka. Both are indicators of aridity.

The evidence for glaciation on land is sparse for this glacial cycle. However, there is evidence in eastern Russia that the Samarovo glaciation dates from MIS 8. In the western Siberian Plain and also the Central Siberian Plateau the Samarovo glaciation was consistently much more extensive than the later Taz glaciation, which is thought to date from later in the Saalian Stage in MIS 6 (Astakhov et al., 2016). Given the scale of the land areas involved, these Siberian ice masses would have been major contributors to global ice volume.

In northwest Europe, the evidence for the MIS 8 glaciation is limited. Recent research from eastern England has argued for extensive MIS 8 glaciation (White et al., 2017). Similarly, Beets et al. (2005) argued that tills in the southern North Sea are MIS 8 in age, based on measurements of the isoleucine epimerisation of mollusc shells and foraminiferal tests. However, throughout the region, no unequivocal physical evidence of glaciation during this interval has been identified, and questions remain as to the real extent of ice over northwestern Europe at this time. By contrast, ice advanced across Poland and the Baltic states, reaching the south Polish uplands (Marks, 2011). Toucanne et al. (2009) showed that fluvial drainage through the English Channel during the MIS 10 and MIS 8 glaciations was significantly less than during MIS 6 and MIS 2. They attribute this difference to massive glacial meltwater drainage associated with much larger glaciations in MIS 6 and 2 compared to MIS 10 and 8.

In the mid-latitude mountains, glaciation dating to MIS 8 is sometimes reported (e.g., in the Italian Apennines; Giraudi and Giaccio, 2017). In Montenegro, Hughes et al. (2011) dated moraine using U-series dating and found evidence for moraines predating MIS 6 yet post-dating older moraines ascribed to MIS 12. The presence of MIS 7 calcites within these moraines led Hughes and coworkers to tentatively suggest a MIS 8 age for the moraines, although they noted that in other valleys the MIS 6 glaciation was larger. Variations in the extents of mountain glaciers as a result of local topoclimatic controls is likely to complicate the glacial sequence at local scales, unlike for larger ice sheets, where the wider regional climate pattern drives glacier mass balance. However, in key mid-latitude mountains in the Southern Hemisphere, such as in Tasmania, what were previously thought to be MIS 8 moraines are now known to be older (Augustinus et al., 2017). So caution must be given to any tentative ages suggesting MIS 8 glaciation.

MIS 11–10 (terminations V to IV)

MIS 10 has a classic asymmetrical pattern in the marine isotope record (Fig. 2). The glacial cycle has a similar structure to MIS 12 but is less severe, with higher global sea levels (Table 1). The marine isotope record does not indicate major double-glaciation patterns exhibited in other glacial cycles and, unlike some glacial cycles, does not have pronounced interstadial conditions mid-cycle. However, the dust record from Antarctica does indicate two major dust peaks, one at ca. 342–341 ka corresponding to the "glacial maximum" indicated in the marine isotope record and another even larger dust peak earlier in the glacial cycle at ca. 355 ka. The latter occurs in substage MIS 10b, which is associated with the coldest part of MIS 10 recorded in global SSTs and also the lowest atmospheric CO_2 levels (Figs. 1 and 2). This asynchrony and offset between the composite marine isotope record (as a record of both ice volume and SSTs) and decoupled global SSTs is ca. 25 ka for this glacial cycle.

Solar radiation in the Northern Hemisphere was lowest late in the glacial cycle, close in time to the glacial maximum indicated in the marine isotope record. Before this, insolation is relatively high and sustained at >480 W m^{-2}, with only minor troughs earlier in the glacial cycle, except for a more significant trough at the MIS 11c/11a boundary that marks the beginning of the glacial cycle.

The evidence for MIS 10 glaciation on land is scarce despite it being characterised by one of the severe cold phases recorded in global SSTs and a pronounced event in marine isotope record on a par with other major glaciations. The terrestrial glacial record in Europe is similar to MIS 8, in that MIS 10 was usually a smaller glacial event than MIS 6,

https://doi.org/10.1017/qua.2018.37 Published online by Cambridge University Press

although MIS 10 was smaller than both MIS 8 and 6 in Siberia (Astakhov et al., 2016). In northern Germany, luminescence ages of ice-marginal deposits indicate ice advances during MIS 10 with ages ranging from 376 ± 27 to 337 ± 21 ka (Roskosch et al., 2014). In their paper, Roskosch et al. (2014) argue that MIS 12, 10, 8, and 6 glaciations reached approximately the same position in the Leine Valley and further east in Poland (e.g. Marks, 2011). However, the evidence for MIS 10, and indeed MIS 8 glaciation across wider Europe, remains in question, as the relationships between sand deposits dated using luminescence techniques and glacial extents can often be ambiguous. In the Italian Apennines, $^{36}Ar/^{40}Ar$ dating of tephra within glaciolacustrine deposits has shown that glaciers advanced in the catchment in MIS 10 (Giraudi et al., 2011; Giraudi and Giaccio, 2017.). Elsewhere, in southernmost central Tibet, Owen et al. (2009, 2010) argued that moraines are considerably older than 300 ka and most likely formed during MIS 10 or during an earlier glacial cycle when ice caps expanded during the Naimona'nyi glaciation. This was based on ^{10}Be exposure dating from moraine boulders.

Despite the relatively limited direct evidence of glaciation, global ice volume must have been substantial, because relative sea levels were on a par with MIS 12 (Rabineau et al., 2006). The $\delta^{18}O$ signal also shows that this glaciation was the fifth in terms of magnitude of the last 10 glacial cycles after MIS 16, 12, 6, and 5d–2.

MIS 13-12 (terminations VI to V)

MIS 12 (Elsterian Stage) was one of the most pronounced of all cold stages, with an amplitude and $\delta^{18}O$ maximum only matched by MIS 16. Based on the top 5% of $\delta^{18}O$ values, MIS 12 was the severest glacial cycle. Calculations of detrended global sea levels (Shakun et al., 2015) also suggest that this was one of the largest glaciations in terms of ice volume of the last 10 glacial cycles (Table 1). It was also the coldest of the last 10 glacial cycles recorded in global SSTs (Fig. 1) (Shakun et al., 2015). In addition to the severity of MIS 12, it was the second longest glacial cycle (after the last glacial cycle), with a termination-to-termination length of 109 ka. This is partly because of the prolonged weak preceding interglacial period (MIS 13). The length of MIS 12 itself is relatively short (Table 1), as is the span of glacial inception to glacial termination (Fig. 2), although these measures clearly provide a misleading perspective of the magnitude and length of this glacial cycle. MIS 12 is especially significant, because it was characterised by some of the largest glaciations recorded in the Northern Hemisphere. Relative sea-level minima during this glacial cycle were the lowest of the past 500 ka at more than -150 ± 10 m compared with -102 ± 6 m for MIS 5d–2, 6, and 8 (Rabineau et al., 2006).

The severity of glaciation in MIS 12 is highlighted by the dust peak recorded in Antarctica (Fig. 2), which is very pronounced at the $\delta^{18}O$ maximum (at ca. 435 ka) and represents the greatest dust flux of all the last 10 glacial cycles. The dust record from Antarctica indicates significant aridity in the build-up to the MIS 12 glacial maximum (MIS 12a), with significant dust peaks between 430 and 470 ka in MIS 12c. The intervening interstadial of MIS 12b is characterised by reduced dust flux and lower $\delta^{18}O$ values. Major dust peaks at ca. 434 and 481 ka are associated with major bolide impact events (Narcisi et al., 2007; Misawa et al., 2010), with the 481 ka most obviously standing out from terrestrial dust signal, an event caused by atmospheric disintegration of a $>10^8$ kg projectile that caused continental-scale distribution of ablation debris across Antarctica (van Ginneken et al., 2010). This was soon followed by a steep collapse in global SSTs to the coldest recorded event of the last 10 glacial cycles, which occurred just 5 ka later at 475 ka in MIS 12c (Fig. 1). Significantly, this was not the global glacial maximum of MIS 12, which occurred later at ca. 438 ka in MIS 12a.

Solar radiation in the Northern Hemisphere was at its lowest early in the glacial cycle (at ca. 480–475 ka). Coinciding with this during the glacial inception into MIS 12, the SST in the North Atlantic Iberian margin decreased 5°C from 478 to 473.5 ka (Rodrigues et al., 2011). However, this initial trough in solar radiation was followed by the low-amplitude variations of solar radiation through the glacial cycle, because the amplitude of precession cycles was reduced due to low orbital eccentricity. In fact, the period between 460 and 425 ka was characterised by much lower-amplitude variations in solar radiation compared with many other glacial cycles (Fig. 2),

In continental Europe, the Elsterian Stage glaciation was more extensive than during the Saalian Stage (MIS 6) limits in eastern Germany and Poland, although not in western Germany and the Netherlands. In the Balkans, the largest glaciation has been dated to >350 ka by U-series dating of secondary carbonates within moraines, with the latter then correlated with MIS 12 by correlation with long lacustrine sequences in Greece (Hughes et al., 2005, 2006, 2010, 2011). The Elsterian Stage is equivalent to the Anglian and Okian Stages (MIS 12) in the British Isles and Russia, respectively. The Anglian Stage represents the most extensive recorded glaciation in southeastern England, when ice reached as far as London. In North America, MIS 12 is correlated with the Illinoian D Stage.

MIS 15–14 (terminations VII to VI)

MIS 14 is known to have been characterised by limited ice extent. This is indicated in the marine isotope record, where the maximum $\delta^{18}O$ value of this cold stage was 4.55 at 548 ka, which is the lowest $\delta^{18}O$ value of all the last 10 cold stages (Table 1). Ice volume would have been the lowest of all the last 10 glacial cycles, with global sea levels much higher than in other glacial periods (Table 1). The relatively weak global glaciation associated with MIS 14 has been proposed as a direct cause of the extended interglacial complex of MIS 15–13 (Hao et al., 2015). A similar argument could be proposed for MIS 7, which also has an extended duration and is preceded by a relatively weak glacial cycle

https://doi.org/10.1017/qua.2018.37 Published online by Cambridge University Press

(Fig. 1). Despite this evidence, global SSTs during MIS 14 were as cold as other glacial periods that were characterised by much bigger glaciations (Fig. 1).

The onset of MIS 14 follows a trough in solar radiation between 570 and 565 ka at the end of MIS 15 (Fig. 2B). Hao et al. (2015) noted that MIS 14 is also characterised by a later trough in solar radiation early in the glacial cycle and argued for a southern inception of glaciation that was associated with changes in the Antarctic ice sheets, since MIS 14 is recorded as a severe cold interval in Southern Hemisphere records, but not so in the Northern Hemisphere.

The Antarctic dust signal for MIS 14 is much weaker than for any other glacial cycles, with dust flux <12 mg/m^2/a. A double-peak pattern is evident at ca. 540 and 530 ka, with the first peak larger than the second (Fig. 2B).

There is little direct evidence of glaciation on land from MIS 14, probably because it was limited in extent compared to later glaciations. However, there are some rare accounts of indirect evidence for glaciation in this interval. In the Italian Apennines, there is evidence that MIS 14 was characterised by significant mountain glacial advances based on evidence recorded in a sediment basin immediately downvalley of glaciated uplands. Here, a glacier advance has been dated to MIS 14 by applying ^{36}Ar/^{40}Ar dating to tephra deposits in a pro-glacial lacustrine sequence in the Campo Felice Basin (Giraudi et al., 2011).

MIS 17–16 (terminations VIII to VII)

MIS 16 was a major cold phase, recording one of the greatest signals of global ice volume with maximum δ^{18}O values equal to MIS 12 (Table 1). However, when SSTs are decoupled from the δ^{18}O record, then MIS 16 appears less severe and no colder than MIS 14 (Fig. 1). Yet the lower quartile value of global sea-level reconstructions (Shakun et al., 2015) suggests that global ice volume was on a par with some of the largest glaciations in other glacial cycles (Table 1). MIS 16 was characterised by two major dust peaks, successively larger at 670–660 and 640–630 ka (Fig. 2B). These dust peaks are separated by a period of warming over Antarctica. However, depressed global SSTs were sustained between both these dust peaks, with the coldest temperatures reached at 650 ka (Fig. 1). Solar radiation is marked by a strong minimum early in the glacial cycle (690–680 ka) (Table 2).

In Europe, MIS 16 is associated with the Don glaciation (Donian Stage; "Cromerian Complex" Stage, glacial c). This was substantially less extensive than the Saalian Stage (MIS 6) and Elsterian Stage (MIS 12) glaciations in western and central Europe. The British and Fennoscandian Ice Sheets terminated in the central North Sea basin in MIS 16 (Lamb et al., 2016). However, MIS 16 was marked by the most extensive glaciation of the southern Russian Plain, with an ice lobe reaching into the Don Valley between Moscow and Volgograd, sourced from both Fennoscandia and Novaya Zemlya. In North America, Bierman et al. (1999) provided cosmogenic ^{10}Be/^{26}Al exposure ages consistent with glaciation during MIS 16 from eroded quartzite surfaces associated with some of the southernmost extensions of the Laurentide Ice Sheet in Minnesota. In the Southern Hemisphere, evidence for MIS 16 glaciation is also recorded in cosmogenic exposure ages in Tasmania (Fink and Augustinus, 2010).

Table 2. Solar radiation peak-trough amplitude at 60°N early in glacial periods or at the end of preceding interglacial periods. Solar radiation data are derived from Berger and Loutre (1991) and Berger (1992). Marine isotope ages are from Lisiecki and Raymo (2005).

	Peak	Age (ka)	Trough	Age (ka)	Amplitude change
MIS 5e/5d–2	544.69	127	440.2	116	104.49
MIS 7/6	531.96	198	443	187	88.96
MIS 9/8	517.25	313	459.83	303	57.42
MIS 11/10	508.45	373	484.84	363	23.61
MIS 13/12	525.83	486	456.22	475	69.61
MIS 15/14	546.62	579	456.09	566	90.53
MIS 17/16	534.77	693	448.99	682	85.78
MIS 19/18	519.22	788	469.87	778	49.35
MIS 21/20	533.87	866	457.08	854	76.79
MIS 23/22	557.44	958	449.54	947	107.90

MIS 16 was characterised by very low CO_2 atmospheric concentrations, the lowest of the last eight glacial cycles, with values below 180 ppm for 3 ka during MIS 16 (Lüthi et al., 2008). This is attributed to pronounced oceanic carbon storage at this time. Major ice-rafting is recorded in North Atlantic sediments during MIS 16 at ~640 ka, and Hodell et al. (2008) suggest that this represents the onset of Heinrich events in this region and the initiation of catastrophic surging of the Laurentide Ice Sheet. This is consistent with the global large ice volume indicated in the marine isotope record for this glacial cycle, since this record is dominated by the Laurentide Ice Sheet (Hughes et al., 2013).

MIS 19–18 (terminations IX to VIII)

MIS 18 spans 60 ka and contains two distinct glacial periods in the marine isotope record. These are MIS 18a and 18e, with the largest δ^{18}O trough being in the later MIS 18a (Figs. 1 and 2B). However, the Antarctic ice-core dust record shows a much larger peak in MIS 18e (28 mg/m^2/a) compared with 18a (15 mg/m^2/a). An unusually large dust peak at 743 ka (46 mg/m^2/a) is unlikely to be terrestrial dust and preceded the dust peak in MIS 18e by ca. 1.7 ka. It is likely that the 743 ka dust peak is associated with a meteoritic event like those that occurred at 434 and 481 ka (cf. MIS 12). MIS 18e is also characterised by colder global SST than the later MIS 18a.

The δ^{18}O trough value of 4.75 at 718 ka is close to the median of the last 10 cold stages (Table 1), and the lower quartile value of global sea levels is higher than all other following glacial periods but lower than MIS 14 and 8. A notable characteristic of this glacial cycle is also the

https://doi.org/10.1017/qua.2018.37 Published online by Cambridge University Press

strong interstadial of MIS 18b–d. This represents the largest amplitude in $\delta^{18}O$ variation within any of the last 10 glacial cycles. Peak amplitude can be defined as the difference in $\delta^{18}O$ values between the peak of the substage (MIS 18c) and the smallest of the troughs either side (MIS 18e). This is only matched by MIS 9a and 23c. The interstadial of MIS 18b–d is also very prominent in the EPICA ice-core temperature record and is characterised by a 5°C amplitude peak.

MIS 18 is one of only three glacial cycles that do not have a major trough in Northern Hemisphere insolation early in the glacial cycle or at the end of the preceding interglacial period. The largest solar minimum in MIS 18 occurs late in the glacial cycle, close to the glacial maximum indicated in the marine isotope record. The warm interstadial of MIS 18b–d is characterised by an insolation peak.

As with MIS 14 (discussed earlier) and MIS 20 (discussed in the following section), there is little direct evidence of glaciation on land in MIS 18. Head and Gibbard (2015) noted that this implies that later glaciations were more extensive and therefore probably destroyed evidence for these events, but also that some of these glacial deposits have been inadequately differentiated owing to the limitations of current dating techniques. However, MIS 18 is represented on the Russian Plain by the Setun Till (and equivalents), during which ice expanded from Scandinavia as far south as the Tula region (Velichko et al., 2004). It is related to 'glacial b' of the 'Cromerian Complex' Stage. In China, the Wangkun glaciation, the oldest in the Kunlun Shan Pass, was dated at 710 ka using electron spin resonance. This is similar to the ^{36}Cl age of the bottom ice layer of a 309 m ice core of the Guliya Ice Cap, western Kunlun Shan. These ages coincide with MIS 18 and suggest ice build-up at this time (Zhou et al., 2006).

MIS 21–20 (terminations X to IX)

MIS 20 was the second shortest cold stage of the last 10 glacial cycles, with a span of 55 ka. In terms of ice volume, the marine isotope $\delta^{18}O$ value was close to the median of the last 10 glacial cycles (Table 1). MIS 20 was preceded by a major Northern Hemisphere insolation minimum in MIS 21 at ca. 854 ka. The amplitude of solar flux declines through the following glacial cycle of MIS 20 (Figs. 2B and 4).

In Europe, MIS 20 is equated to 'glacial a' of the 'Cromerian Complex' Stage. Little or no evidence of glaciation during this event is known. However, according to Velichko et al. (2004), Fennoscandian ice expanded during this event as far south as Moscow, where till is attributed to the Likovo glaciation. Possible limited glacial extent elsewhere is implied by finds of erratic clasts in fluvial sediments in Europe (e.g. Clark et al., 2004). Oceanic evidence of warm waters in the North Atlantic off-Iberia during MIS 20 and 18 indicate that atmospheric moisture derived from this warm water might have been advected deep into continental Europe and contributed to enhanced growth of Alpine glaciers (Bahr et al., 2018).

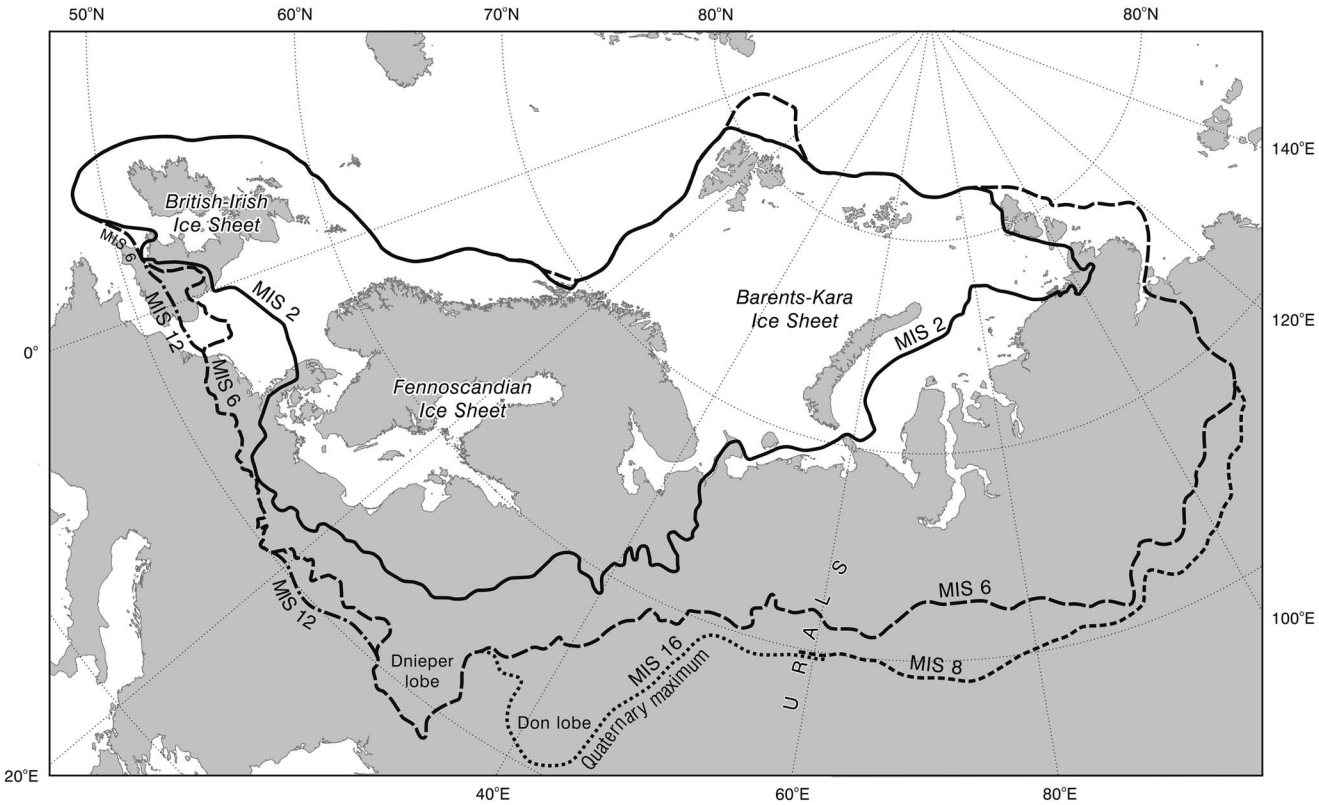


Figure 4. Limits of the Eurasia contiguous ice sheets during the middle and late Pleistocene. Adapted from information in Svendsen et al. (2004), Ehlers and Gibbard (2004), and Astakhov et al. (2016).

https://doi.org/10.1017/qua.2018.37 Published online by Cambridge University Press

MIS 23–22 (terminations XI to X) or 25–22 (terminations XII to X)

MIS 24–22 is important for considering global glaciations, because it has been identified by some as the first of the 100 ka cycles following the mid-Pleistocene Transition. It includes MIS 23, which some describe as an interglacial period (e.g., Pena and Goldstein, 2014), whereas others consider MIS 22–24 to represent a long, single, glacial cycle, the first prolonged 100 ka cycle (e.g., Elderfield et al., 2012). When $\delta^{18}O$ values are compared with other glacial records, then MIS 23 does not have the magnitude of later interglacial periods (Fig. 1). Thus, the glacial cycle can be defined as the interval between terminations XII to X. On the basis of this subdivision, the glacial cycle represents the second-longest cold stage of the last 10 glacial cycles (after the last glacial cycle) when defined based on marine isotope stages and the equal second longest when defined from termination to termination (Table 1). MIS 24–22 is characterised by some significant changes in drivers of environmental change. The amplitude of solar insolation in the Northern Hemisphere in the downturn to MIS 24 was the largest of all the glacial cycles (Fig. 4, Table 2). MIS 22–24 was also a period of marked global CO_2 reduction (Hönisch et al., 2009) and saw major Antarctic ice expansion (Elderfield et al., 2012). This cold stage was also marked by a significant change in the global ocean thermohaline circulation system, which became much weaker in this glacial cycle than in earlier glacial periods (Pena and Goldstein, 2014).

Preservation of surface glacial evidence for such an old glaciation is obviously rare, but major glaciation is recorded indirectly in several contexts. In the Italian Dolomites, glaciation became established during MIS 22 (Muttoni et al., 2003). Large-scale glaciation is first seen in North America in MIS 22 (Barendregt and Duk-Rodkin, 2011; Duk-Rodkin and Barendregt, 2011). In Pennsylvania, the most extensive glacial record is attributed to MIS 22 or older (Braun, 2011) and presents a rare example of how the lateral extent of this glaciation was possibly greater than all later glaciations. The transition to a thicker Laurentide Ice Sheet around this time (~950 ka) has been attributed to a change in subglacial conditions caused by earlier ice sheet removal of thick regolith (Clark and Pollard, 1999). However, a substantial increase in ice volume through the mid-Pleistocene Transition was a global phenomenon. For example, in the Southern Hemisphere, in Tasmania, the Bulgobac glaciation—the most extensive on this island—has been dated to 890–783 ka using magnetic polarity (Augustinius and Macphail, 1997); this time period encompasses MIS 22 and 20.

CONTROLS AND DRIVERS OF GLACIAL CYCLES

Solar forcing and CO_2

Solar forcing of global climate in response to orbital variations has been the established paradigm for understanding the pacing of glacial cycles for over 40 years (e.g., Hays et al., 1976). However, the relationship between solar forcing and global glacier behaviour is less well established. Within glacial periods, precessional cycles and the seasonal patterns of solar receipt exert important controls on global ice volume, with deglaciations triggered every fourth or fifth precessional cycle (Ridgwell et al., 1999). Glacier ablation is largely driven by summer temperatures, which is directly influenced by summer insolation. Thus, variations in the latter through glacial cycles are likely to have a profound impact on glacier mass balance. This has important implications for not only deglaciations but also glacier build-up at glacial inceptions.

Many of the glacial cycles with the biggest recorded glaciations saw the lowest Northern Hemisphere insolation during the glacial inception at the end of the preceding interglacial period. This was the case for MIS 5d–2, 6, 8, 12, 14, 16, 20 and 24–22. MIS 18 and 10 are both preceded by solar troughs, but this is exceeded later in the cold stage. The fact that many of the major cold stages begin with a major trough in insolation in the Northern Hemisphere suggests that glacial inception and the significant build-up of glaciers starts in the Northern Hemisphere. This is because of the much larger land area in this hemisphere. Furthermore, the build-up and collapse of ice sheets over the Northern Hemisphere, especially over North America, dominate the ice volume signal in the global $\delta^{18}O$ record. This is compounded by the fact that there has been comparatively little change in ice volume over Antarctica between some glacial and interglacial periods (e.g., Lilly et al., 2010; Hughes et al., 2013; Joy et al., 2017).

Ganopolski et al. (2016) highlighted the importance of CO_2 in glacial inception. They identified points in time when low CO_2 corresponded with low insolation as potential triggers for global ice build-up. This theory argues that low insolation alone cannot explain the inception of global glacial inception. Instead, it is the combination of insolation forcing with atmospheric CO_2 concentrations that drives glacial inceptions. Nevertheless, the troughs in insolation in the high northern latitudes all coincide with the points in time identified by Ganopolski et al. (2016) as favourable for glacial inception.

The relationship between Northern Hemisphere solar radiation and global sea levels is illustrated in Figure 5 for glacial cycles defined by both MIS boundaries (A) and when defined by termination to termination (B). Global sea-level minima are summarised by the lower quartile of detrended global sea-level data provided in Shakun et al. (2015). Absolute minima from this data set are not used, because the sea-level values only represent approximate estimates. Nevertheless, a medium-strong relationship can be observed when comparing the sea-level data with solar radiation (Fig. 5). This shows that there is a statistically significant relationship between the lowest quartile or decile June solar radiation at 60°N and global sea levels as recorded in the lower quartile of detrended sea level in the global stack of Shakun et al. (2015). The strongest relationships are seen when using the lower-quartile solar radiation values for the shorter MIS glacial definitions (i.e., MIS 5d–2, 6,

https://doi.org/10.1017/qua.2018.37 Published online by Cambridge University Press

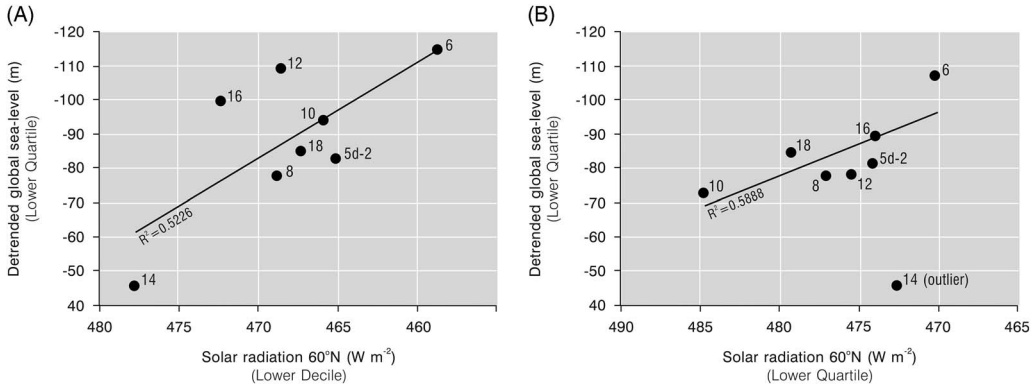


Figure 5. Regression between mean Northern Hemisphere solar radiation (at 60°N) and the sea levels detrended from the $\delta^{18}O$ record for the last eight glacial cycles using solar radiation data from Berger and Loutre (1991) and Berger (1992) and detrended sea-level data from Shakun et al. (2015). (A) Glacial cycles defined using the marine isotope stage boundaries (i.e., MIS 5d–2, 6, 8, 10, 12, 14, 16, 18). (B) Glacial cycles defined by termination to termination; MIS 14 is excluded from the regression trend line calculation. The relationships are statistically significant for trend lines shown in (A) and (B), where *p*-values are 0.0427 and 0.0440, respectively.

8, etc.) and when using the lower-decile solar radiation values for the longer termination-to-termination definitions. The strength of the relationships ($R^2 = 0.5226$ and 0.5888) indicates that just over half of global sea-level change may be explained through variations in Northern Hemisphere solar radiation. The explanation being that solar radiation drives global ice volume, which then drives global sea-level change. The rest of the variation in global sea-level change, unaccounted for by solar variations, must also be down to other factors, although still largely related to global ice dynamics and global temperatures. A striking outlier in the relationship when considering the termination-to-termination interval is MIS 14, which is excluded from the regression trend line in Figure 5B. This suggests that this marine isotope stage does not conform to the pattern of other orbitally driven glacial cycles.

The correlations between global sea level and solar radiation highlights the importance of internal controls on glacier–climate dynamics in controlling the nature of glacial cycles. Almost all theories of ice ages feature a phenomenon of synchronisation between internal climate dynamics and astronomical forcing (Crucifix, 2012). However, whilst solar forcing is clearly important in glacial inceptions (this paper) and also for the prediction of glacial inceptions and interglacial periods (Ganopolski et al., 2016; Tzedakis et al., 2017), there should not be too much emphasis placed on solar forcing as a driver of global glacier dynamics *within* glacial cycles.

The first of the 100 ka glacial cycles is marked by the cold interval of MIS 24–22. This cold stage was preceded early in the glacial cycle by the largest amplitude change (from peak to trough) in insolation in the Northern Hemisphere of the last million years. The second-largest amplitude change in insolation (from peak to trough) of the last million years occurred at the start of the last glacial cycle (MIS 5d–2). Significantly, both MIS 5d–2 and MIS 24–22 were the longest of the last 10 glacial cycles, hinting at a causal relationship between insolation amplitude changes at the beginning of glacial cycles and the glacial-cycle length. Whether the trough in insolation is at the end of the preceding interglacial period or at the start of the glacial period is not significant. This is partly because glacial–interglacial boundaries are relatively arbitrary constructs and, more significantly, because glaciers can form today in relatively warm conditions so long as snow accumulation is great enough (e.g. Hughes, 2008, 2009). The key is to provide a kick-start to glacier expansion via reduced summer melting at a time of sustained winter precipitation. The fact that MIS 25/24 saw the largest amplitude changes in solar radiation from peak to trough at both 60°N and 30°N, whereas for MIS 5e/5d the 30°N was much less than at 60°N, suggests that for the former the mid-latitudes were more affected. This is likely to have caused early glacier expansion in MIS 24–22 not just in high-latitude Asia, such as Siberia, as was the case for the last glacial cycle, but also in central Asia in places like the Altai, the Tien Shan, and the Tibetan Plateau.

It is possible that the first 100 ka cycle was driven by global glacier behaviour and associated climate feedbacks, with MIS 24–22 looking very much like MIS 5d–2 and MIS 23 analogous to MIS 3 (Figs. 1 and 2). Both MIS 5–2 and MIS 24–22 were characterised by an early glacier maxima in Asia (driven by a large insolation trough at the end of the preceding interglacial period), that was then followed by glacier advances spreading out to the maritime margins around the Atlantic (as climate cooled) for the second half (and maximum) of the glacial cycles. This effect prolongs the glacial intervals as first the Eurasian continental glaciers grow, then recede as climate becomes too dry, whilst the maritime-driven ice sheets around the North Atlantic continue to grow and dominate the world's ice-volume record.

Another important consideration is the effect of precession on the melt season. During the last glacial cycle, the effects of precession decline through the glacial cycle. This means that the lengthening of the melt season during upswings to solar peaks becomes diminished. This is characteristic of most glacial cycles, and the resulting excess ice build-up causes ice sheet instability and ultimate collapse during terminations after the fourth or fifth precessional cycles (Raymo, 1997; Ridgwell et al., 1999).

https://doi.org/10.1017/qua.2018.37 Published online by Cambridge University Press

Geographic location

The pattern of solar radiation receipt in the Northern Hemisphere has a close relationship to the pattern of Antarctic air temperatures (Fig. 2). This implies a Northern Hemisphere role in driving global climate over the last ten 100 ka glacial cycles. Whilst Miocene ice build-up in Antarctica is likely to have been enabled by changing continental configurations in the Southern Hemisphere (e.g., Scher and Martin, 2006), for the last 800 ka there are clear links observed between climate changes in the Greenland and Antarctic ice-core records (EPICA, 2006; Jouzel et al., 2007a). The thermal bipolar seesaw, whereby climate changes in the Northern and Southern Hemispheres are closely linked, albeit asynchronously at millennial time scales, is often attributed to oceanographic controls (Shackleton et al., 2000; Stocker and Johnsen, 2003; Stenni et al., 2011). However, whilst Shackleton et al. (2000) noted that the planktonic $\delta^{18}O$ record off Portugal closely matched the Greenland ice-core records, the benthic $\delta^{18}O$ record was in phase with the temperature record from the Vostok ice core in Antarctica. This led Shackleton et al. (2000) to suggest that Antarctic temperatures changes as a result of global ice volume, which, as highlighted in the previous section, is dominated by events in the Northern Hemisphere.

Rohling et al. (2017) highlighted the contrast in global ice distributions between the PGM and the LGM, with Eurasia displaying much larger ice volume during the former compared with the latter. This situation is likely to be partly driven by wetter conditions over Eurasia during MIS 6, a situation enabled by warmer global oceans (Fig. 1). This illustrates how geographic variations in the effects and strengths of oceanic/maritime influences on land can cause major differences in global ice distributions. However, whilst global ocean temperature patterns are likely to affect global glacier distributions, there is evidence, for the early Pleistocene at least, that the role of ice sheets themselves in controlling global air and ocean temperatures may be more limited (cf. Shakun, 2017).

Continentality affects glacier build-up and development in three ways. First, continental interiors are more sensitive to changes in solar radiation receipt than maritime areas. Land masses have a lesser heat capacity than the oceans, resulting in greater sensible and latent heat flux over the former in response to increased solar radiation. Second, moisture supply to continental areas is strongly affected by the prevailing synoptic conditions, especially the development of blocking anticyclones. The first effect essentially controls temperatures, whilst the second controls precipitation—both fundamental factors in glacier mass balance. A third effect of continentality is on the response of glacier mass balance to changes in temperatures. For example, cold and dry glaciers are less sensitive to a change in air temperatures than warm and wet glaciers (Braithwaite and Raper, 2007). This is important, because it means that, once established, continental glaciers will be less sensitive to climatic cooling than maritime glaciers. Continental glaciers are therefore not as sensitive to temperature effects compared with the effects of moisture supply. This third point therefore implies that it is moisture supply to the continental interiors that will ultimately drive glacier behaviour in these regions through glacial cycles. So, with respect to glacier mass balance, it is likely that the effect of solar radiation changes on seasonal distribution of precipitation (accumulation) is likely to be more significant than the relationship between solar radiation and summer temperatures (ablation). Furthermore, the supply of moisture to Arctic Asia would require an open Arctic Ocean, a situation that is much more likely early in a glacial cycle during the preceding interglacial periods.

The effect of early glacier advances in Arctic Asia and in mid-latitude interior mountain chains (cf. Hughes et al., 2013 and references therein) may explain the first prominent dust flux recorded over Antarctica. This indicator of global aridity is likely to have caused continental and mid-latitude glaciers to retreat. This is also enhanced by notable mid-cycle warming events recorded in Antarctica in many of the glacial cycles. In northeast Asia, the climate was warm and wet in summer at the global LGM (Meyer and Barr, 2017). Winters would have been severe, however, with extensive sea ice over the north Pacific inhibiting moisture availability in winter. Dry cold winters and warm wet summers are the least favourable combination for glacier development, and this may explain why glaciers were restricted in size over northeast Asia in the middle to later parts of the last cold stage (i.e., through MIS 3 and 2).The larger ice sheets at the oceanic margins are able to continue growing, as moisture supply is likely to be sustained through these interstadial conditions, as has been indicated in tree populations at mid-latitude locations for multiple glacial cycles (e.g., Fletcher et al., 2010, 2013; Roucoux et al., 2011). However, once ice masses reach a size sufficient to affect not only regional but global climate, then global aridity reaches its maximum late in the glacial cycle at the global glacial maxima. This is represented by a second prominent dust peak in all glacial cycles. For four of the last eight cold stages (MIS 16, 12, 6, 5d–2), which include some with the largest ice volumes, the second peak in dust flux is larger than the first. This pattern is reversed in MIS 8, 10, 14 and 18, which includes cold stages with the smallest ice volume. This may indicate that the early glacier advances in the continental interiors were the largest of the glacial cycles and not subsequently matched by significant glacier expansion in the oceanic margins. This is supported by the fact that some of the largest glaciations in Siberia occurred in MIS 8 (Astakhov et al., 2016), when overall this cold stage was one of the least significant of the last ten glacial cycles in terms of ice volume. This phenomenon can also be invoked to explain why in both MIS 8 and 10 global CO_2 is lowest in the first major ice advance and higher in the second and at the global glacial maxima indicated in the ice volume record (Fig. 2).

Glacier size is important because of the effects of this on the rate of glacier response to climate changes (Bahr et al., 1998). Alpine-style mid-latitude mountain glaciers respond more rapidly to climate changes than large ice sheets. This effect is partly interwoven with the climatic setting with small wet-cold

https://doi.org/10.1017/qua.2018.37 Published online by Cambridge University Press

maritime glaciers even more sensitive to climate changes than large dry-cold continental ice sheets. However, once glaciers achieve sufficient size, they can begin to control climate, causing positive feedbacks. Thus, as wet-cold maritime glaciers at oceanic margins grow to form ice caps, then ice sheets, and eventually submerge mountains, the climatic setting of these glaciers will morph from cold-wet maritime to dry-cold continental. In the process, the latter become less sensitive to changes in air temperature, as noted earlier (cf. Braithwaite and Raper, 2007). This may explain why the large ice sheets around the oceanic margins are able to persist and maintain growth late into the glacial cycle. Moisture-driven maritime glaciers are more likely to survive increased global aridity as glacial cycles persist, and by the time mid-glacial interstadial conditions are reached, as occurred in many glacial cycles, these glaciers have achieved ice sheet status. This has been confirmed through modelling for MIS 3, for example (Arnold et al., 2002). If glaciers at oceanic margins have not achieved this size by mid-cycle, then it is possible that this explains why maximum ice volume is more limited in some cold stages than in others (i.e., MIS 8 and 14).

PROBLEMS AND PROSPECTS IN THE STUDY OF GLACIATIONS AND GLACIAL CYCLES

Southern Hemisphere glaciations and earlier 41 ka glacial cycles

This paper emphasises the role of the Northern Hemisphere in forcing global glaciations and concentrates on the last ten glacial cycles. This inevitably biases the study against the possibility of Southern Hemisphere glacial-forcing mechanisms and earlier 41 ka cycles. For example, the biggest glaciations recorded on land in places like Patagonia occurred at 1.1 Ma during MIS 30–34 (Rabassa et al., 2005). Understanding the drivers of earlier glacial cycles requires further research, and it is not necessarily to be expected that the drivers of the last ten 100 ka glacial cycles can explain the patterns of earlier 41 ka glacial cycles.

Differences between individual glacial cycles as artefacts of larger 400 ka mega-glacial cycles

Figure 6 shows the moving average at 50 ka step intervals of the global marine isotope record for the past million years. This shows that the biggest amplitude variations between glacial and interglacial periods occurred during the past 450 ka. Lang and Wolff (2011) made a similar observation in their study of glacial cycles, noting that strong interglacial periods are confined to the last 450 ka. However, whilst Figure 5 also shows that the largest glaciations are also confined to the past 450 ka, the phase change occurred earlier, at ca. 630 ka. Whilst the onset of 100 ka glacial cycles is often placed with MIS 24–22, Figure 6 shows that a distinct transition to the large-amplitude 100 ka glacial cycles can be identified after MIS 16. Global ice volume fluctuations therefore appear to lag the mid-Pleistocene Transition between 1.25 and 0.5 Ma (Head and Gibbard, 2005). Mudelsee and Schulz (1997) recognised this lag and suggested the onset of 100 ka cycle lags ice volume build-up by 280 ka, with an increase in amplitude at 641 ka. This is consistent with the large amplitude of MIS 16, and when examining glacial cycles in terms of 50 ka moving average (half the 100 ka cycle), then it becomes apparent that an abrupt change in glacial amplitude starts around this time (Fig. 6). The 50 ka moving average in Figure 6 shows that glacial periods became steadily stronger until MIS 16, and this was then followed by the prolonged interglacial/weak glacial complex of MIS 15–14–13. It is notable that it is not only some glacial periods that become longer and greater in amplitude after MIS 16, but interglacial periods become longer and greater in amplitude as well. In fact, the nature of preceding interglacial periods appears to affect the structure of some succeeding glacial periods, especially the weaker glacial periods encompassing MIS 14 and 8. The significance of MIS 12 in Figure 6 as one of the most pronounced glaciations is likely to be related to unique solar patterns, as noted earlier, with an initial trough in solar radiation that was then followed by the low-amplitude variations of solar radiation through the glacial cycle (Fig. 2B). This phase of low precession associated with minimum

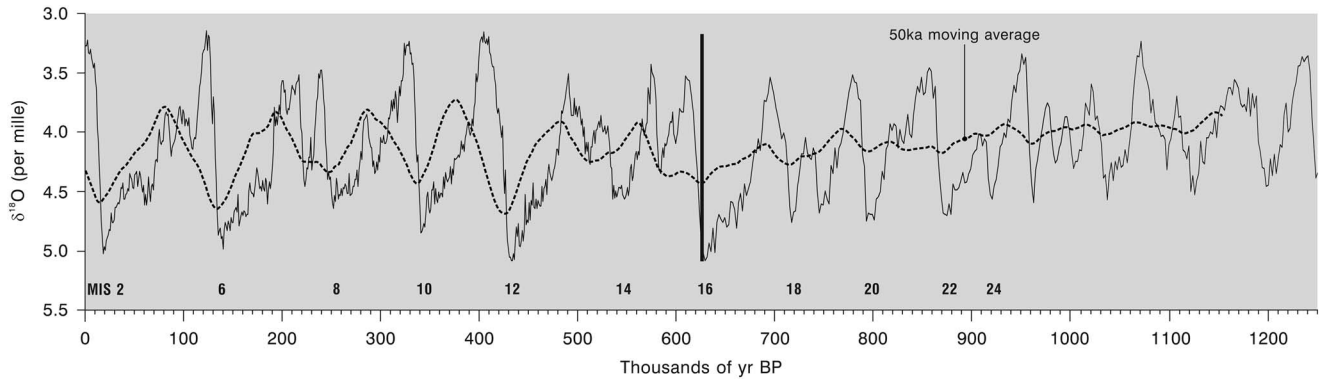


Figure 6. The 50 ka moving average (dashed line) of $\delta^{18}O$ in the global stack (thin black line) for Lisiecki and Raymo (2005). The interval of 50 ka is chosen, as this is half the theoretical 100 ka cycle. Increasing trends towards 100 ka cycles are illustrated by larger amplitudes in the 50 ka moving average of $\delta^{18}O$ values. The vertical bold line marks the phase change from subdued 100 ka cycles to larger-amplitude 100 ka cycles from MIS 16 onwards.

https://doi.org/10.1017/qua.2018.37 Published online by Cambridge University Press

eccentricity towards the end of the 400 ka cycle (minimum at ~438–373 ka; Berger and Loutre, 1991; Laskar et al., 2004) may have enabled ice sheets to expand dramatically during this glacial cycle. This is because lower precession diminishes the contrasts between winter and summer and so inhibits melting during the latter. This is potentially significant, since it hints at 400 ka glacial cycles that are modulated at 100 ka cycles, a pattern noted by Rial (1999).

CONCLUSIONS

The onset of glaciations within the last ten glacial cycles was driven by low solar radiation over Northern Hemisphere high latitudes with rapid glacier advance over the largest high-latitude land masses such as Asia. The driving solar forcing is likely to have been facilitated in conjunction with CO_2 levels, with critical combinations required to cause glacial inception. This phenomenon of glacial inception can be recognised as a global hydrological event and is marked by early dust peaks in Antarctic ice-core records. In most glacial cycles, ice continued to build up in land areas bounded to the west by oceanic margins, such as the North Atlantic (British–Irish and Scandinavian ice sheets) and North Pacific (Cordillerran and Laurentide Ice Sheets). Whilst these ice masses grew, global climate became drier, resulting in a second and usually the most pronounced dust peak of glacial cycles recorded in Antarctic ice cores. Asian glaciers are likely to have retreated at this time.

The analogue for this scenario is the last glacial cycle, for which many glacier records are now well dated. MIS 24–22, the first cold episode of the 100 ka cycles, is very similar in structure to MIS 5d–2, especially in terms of its length and two-phase structure. Furthermore, MIS 24–22 was preceded by the largest amplitude drop in Northern Hemisphere solar radiation of all the last ten glacial cycles. As with the last glacial cycle, this would have caused early, rapid, and extensive Asian glacier expansion, and the intensity of this solar trigger may partly explain the length of the first 100 ka glacial cycle. Whilst common spatial and temporal patterns of glacier build-up and decay can be identified in four of the last eight glacial cycles, MIS 18, 14, 10 and 8 appear different. These were characterised by a more pronounced early dust peak in Antarctica compared with the second later peak, and this is attributed to weaker later oceanic margin glaciation, which usually occurs at the height of glacial cycles, in contrast to the early Asian advances.

Whilst solar radiation played an important role in glacial inceptions, it accounts for only about half of the variability in global ice volume magnitude during the last ten glacial cycles. The other half must be attributed to internal global climate dynamics, including the effects of glaciers themselves on the global climate system. In this respect, once ice sheets become sufficiently large, they exert feedback effects on the global climate system. Whilst glacier feedback mechanisms are well known as an explanation for the terminations of glacial cycles, this paper shows that glacier–climate feedbacks also influence the spatial and temporal patterns of global glaciations during glacial cycles.

ACKNOWLEDGMENTS

We would like to thank Doug Benn and an anonymous reviewer for their rigorous and very helpful reviews, and also the QR Associate Editor Jamie Shulmeister and QR Editor Lewis Owen for their comments on an earlier draft of this paper. The editorial process has greatly improved and refined our original ideas, and this is sincerely appreciated. We thank Bruce Railsback (University of Georgia) for helpful advice and comments on the subdivision of cold stages within glacial cycles; William Fletcher (University of Manchester), who provided some critical insight into the structure of glacial cycles; and also Chronis Tzedakis and Mark Maslin (University College London) for insightful discussion on glacial cycles and for pointing us in some useful directions. We thank Graham Bowden for drawing all the figures.

REFERENCES

Arnold, N. S., van Andel, T. H., Valen, V., 2002. Extent and dynamics of the Scandinavian ice sheet during Oxygen Isotope Stage 3 (65,000–25,000 yr BP). *Quaternary Research* 57, 38–48.

Arrhenius, G., 1952. *Sediment Cores from the East Pacific. Reports of the Swedish Deep-Sea Expedition 1947–1948*. Vol. 5. 227 pp. Swedish Natural Science Research Council, Stockholm.

Astakhov, V., 2004. Pleistocene ice limits in Russian northern lowlands. In: Ehlers, J., Gibbard, P.L. (Eds.), *Quaternary Glaciations—Extent and Chronology*. Part 1, *Europe*. Elsevier, Amsterdam, pp. 309–319.

Astakhov, V., 2018. Late Quaternary glaciation of the northern Urals: a review and new observations. *Boreas* 47, 379–389. doi: 10.1111/bor.12278.

Astakhov, V., Shkatova, V., Zastrozhnov, A., Chuyko, M., 2016. Glaciomorphological map of the Russian Federation. *Quaternary International* 420, 4–14.

Augustinus, P., Fink, D., Fletcher, M.-S., Thomas, I., 2017. Re-assessment of the mid to late Quaternary glacial and environmental history of the Boco Plain, western Tasmania. *Quaternary Science Reviews* 160, 31–44.

Augustinus, P.C., Macphail, M.K., 1997. Early Pleistocene stratigraphy and timing of the Bulgobac Glaciation, western Tasmania, Australia. *Palaeogeography, Palaeoecology, Palaeoecology* 128, 253–267.

Ayalon, A., Bar-Matthews, M., Kaufman, A., 2002. Climatic conditions during marine isotope stage 6 in the eastern Mediterranean from the isotopic composition of speleothems of Soreq Cave. *Geology* 30, 303–306.

Bahr, A., Kaboth, S., Hodell, D., Zeeden, C., Fiebig, J., Friedrich, O., 2018. Oceanic heat pulses fueling moisture transport towards continental Europe across the mid-Pleistocene transition. *Quaternary Science Reviews* 179, 48–58.

Bahr, D.B., Pfeffer, W.T., Sassolas, C., Meier, M.F., 1998. Response time of glaciers as a function of size and mass balance. *Journal of Geophysical Research* 103, 9777–9782.

Bard, E., Delaygue, G., Rostek, F., Antonioli, F., Silenzi, S., Schrag, D.P., 2002. Hydrological conditions over the western Mediterranean basin during the deposition of the cold sapropel 6 (ca. 175 kyr BP). *Earth and Planetary Science Letters* 202, 481–494.

https://doi.org/10.1017/qua.2018.37 Published online by Cambridge University Press

Barendregt, R.W., Duk-Rodkin, A., 2011. Chronology and extent of Late Cenozoic ice sheets in North America: a magnetostratigraphical approach. In: Ehlers, J., Gibbard, P.L., Hughes, P.D. (Eds.), *Quaternary Glaciations—Extent and Chronology*. Developments in Quaternary Science, Vol. 15. Elsevier, Amsterdam, pp. 419–427.

Beets, D.J., Meijer, T., Beets, C.J., Cleveringa, P., Laban, C., van der Spek, A.J.F., 2005. Evidence for a Middle Pleistocene glaciation of MIS 8 age in the southern North Sea. *Quaternary International* 133–134, 7–19.

Bereiter, B., Eggleston, S., Schmitt, J., Nehrbass-Ahles, C., Stocker, T.F., Fischer, H., Kipfstuhl, S., Chappellaz, J., 2015. Revision of the EPICA Dome C CO2 record from 800 to 600 kyr before present. *Geophysical Research Letters* 42, 542–549. doi: 10.1002/2014GL061957.

Berger, A., 1992. *Orbital Variations and Insolation Database. IGBP PAGES/World Data Center for Paleoclimatology Data Contribution Series #92-007*. NOAA/NGDC Paleoclimatology Program, Boulder, CO. ftp://ftp.ncdc.noaa.gov/pub/data/paleo/insolation/ (accessed May 4, 2018).

Berger, A., Loutre, M.F., 1991. Insolation values for the climate of the last 10 million years. *Quaternary Science Reviews* 10, 297–317.

Bierman, P.R., Marsella, K.A., Patterson, C., Thompson Davis, P., Caffee, M., 1999. Mid-Pleistocene cosmogenic minimum-age limits for pre-Wisconsinan glacial surfaces in southwestern Minnesota and southern Baffin Island: a multiple nuclide approach. *Geomorphology* 27, 25–39.

Blockley, S.P.E., Lane, C.S., Hardiman, M., Rasmussen, S., Seierstad, I., Turney, C.S., Bronk Ramsey, C., 2012. Synchronisation of palaeoenvironmental records over the last 60,000 years, an extended INTIMATE group protocol. *Quaternary Science Reviews* 36, 2–10.

Blunier, T., Chappellaz, J., Schwander, J., Dällenbach, A., Stauffer, B., Stocker, T.F., Raynaud, D., et al., 1998. Asynchrony of Antarctic and Greenland climate change during the last glacial period. *Nature* 394, 739–743.

Braithwaite, R.J., Raper, S.C.B., 2007. Glaciological conditions in seven contrasting regions estimated with the degree-day model. *Journal of Glaciology* 46, 297–302.

Braun, D., 2011. The glaciation of Pennsylvania, USA. In: Ehlers, J., Gibbard, P.L., Hughes, P.D. (Eds.), *Quaternary Glaciations—Extent and Chronology: A Closer Look*. Vol. 15, *Developments in Quaternary Science*. Elsevier, Amsterdam, pp. 521–530.

Broecker, W.S., van Donk, J., 1970. Insolation changes, ice volumes, and the O18 record in deep-sea cores. *Reviews of Geophysics* 8, 169–198.

Capron, E., Vázquez Riveiros, N., He, F., Jacobel, A., Zhang, X., 2016. Spatial pattern and temporal evolution of glacial terminations of the last 800 ka. *Past Global Changes Magazine* 25, 118.

Cheng, H., Edwards, L., Broecker, W.S., Denton, G.H., Kong, X., Wang, Y., Zhang, R., Wang, X., 2009. Ice Age terminations. *Science* 326, 248–252.

Clark, C.D., Gibbard, P.L., Rose, J., 2004. Pleistocene glacial limits in England, Scotland and Wales. In: Ehlers, J., Gibbard, P.L. (Eds.), *Quaternary Glaciations—Extent and Chronology*, Part 1. *Europe*. Amsterdam, Elsevier, pp. 47–82.

Clark, P.U., Pollard, D., 1999. Origin of the middle Pleistocene transition by ice sheet erosion of regolith. *Paleoceanography* 13(1), 1–19.

Cohen, K.M., Gibbard, P.L., 2011. *Global Chronostratigraphical Correlation Table for the last 2.7 Million Years*. Subcommission on Quaternary Stratigraphy (International Commission on Stratigraphy), Cambridge, UK. https://quaternary.stratigraphy.org/correlation/POSTERSTRAT_v2011.pdf.20110222-162627 (accessed May 4, 2018).

Colleoni, F., Wekerle, C., Näslund, J-O., Brandefelt, J., Masina, S., 2016. Constraint on the penultimate glacial maximum Northern Hemisphere ice topography (~140 kyrs BP). *Quaternary Science Reviews* 137, 97–112.

Crucifix, M., 2012. Oscillators and relaxation phenomena in Pleistocene climate theory. *Philosophical Transactions of the Royal Society A* 370, 1140–1165.

Curry, B.B., Grimly, D.A., McKay, E.D. III, 2011. Quaternary glaciations in Illinois. In: Ehlers, J., Gibbard, P.L., Hughes, P.D. (Eds.), *Quaternary Glaciations—Extent and Chronology: A Closer Look*. Vol. 15, *Developments in Quaternary Science*. Elsevier, Amsterdam, pp. 467–488.

Denton, G.H., Hughes, T.J., 1981. *The Last Great Ice Sheets*. Wiley, New York.

De Schepper, S., Gibbard, P.L., Salzmann, U., Ehlers, J., 2014. A global synthesis of the marine and terrestrial evidence for glaciation during the Pliocene Epoch. *Earth-Science Reviews* 135, 83–102.

Duk-Rodkin, A., Barendregt, R.W., 2011. Stratigraphical record of glacials/interglacials in northwest Canada. In: Ehlers, J., Gibbard, P.L., Hughes, P.D. (Eds.), *Quaternary Glaciations—Extent and Chronology*. Vol. 15, Developments in Quaternary Science, Elsevier, Amsterdam, pp. 661–699.

Ehlers, J., Gibbard, P.L., 2007. The extent and chronology of Cenozoic global glaciation. *Quaternary International* 164–165, 6–20.

Ehlers, J., Gibbard, P.L., 2008. Extent and chronology of Quaternary glaciation. *Episodes* 31, 211–218.

Ehlers, J., Gibbard, P.L. (Eds.), 2004. *Quaternary Glaciations – Extent and Chronology*. Developments in Quaternary Science Volume 2, Parts I, II, and III, Elsevier, Amsterdam.

Ehlers, J., Gibbard, P.L., Hughes, P.D., 2011a. Introduction. In: Ehlers, J., Gibbard, P.L., Hughes, P.D. (Eds.), *Quaternary Glaciations—Extent and Chronology: A Closer Look*. Vol. 15, *Developments in Quaternary Science*, Elsevier, Amsterdam, pp. 1–14.

Ehlers, J., Gibbard, P.L., Hughes, P.D. (Eds.), 2011b. *Quaternary Glaciations—Extent and Chronology: A Closer Look* Vol. 15, Developments in Quaternary Science, Elsevier, Amsterdam.

Ehlers, J., Grube, A., Stephan, H-J., Wansa, S., 2011c. Pleistocene glaciations of north Germany—new results. In: Ehlers, J., Gibbard, P.L., Hughes, P.D. (Eds.), *Quaternary Glaciations—Extent and Chronology: A Closer Look*. Vol. 15, *Developments in Quaternary Science*. Elsevier, Amsterdam, pp. 149–162.

Elderfield, H., Ferretti, P., Greaves, M., Crowhurst, S., McCave, N., Hodell, D., Piotrowski, A.M., 2012. Evolution of ocean temperature and ice volume through the mid-Pleistocene climate transition. *Science* 337, 704–709.

[EPICA] European Project for Ice Coring in Antarctica Community Members. 2006. One-to-one coupling of glacial climate variability in Greenland and Antarctica. *Nature* 444, 195–198.

Fairbridge, R.W., 1972. Climatology of a glacial cycle. *Quaternary Research* 2, 283–302.

Fink, D., Augustinus, P., 2010. Glacial history of Tasmania from mid-Pleistocene to the Last Glacial Maximum—new challenges and new ideas for hemispheric glacial climate correlations. In: International Glaciological Conference (VICC 2010)—"Ice and Climate Change: A View from the South," Centro de Estudios Científicos (CECS), Valdivia, Chile, February 1–3, 2010. http://apo.ansto.gov.au/dspace/handle/10238/2881 (accessed May 4, 2018).

Fletcher, W., Sánchez-Goñi, M.F., Allen, J.R.M., Cheddadi, R., Combourieu Nebout, N., Huntley, B., Lawson, I., et al., P.C., 2010.

https://doi.org/10.1017/qua.2018.37 Published online by Cambridge University Press

Millennial-scale variability during the last glacial in vegetation records from Europe. *Quaternary Science Reviews* 29, 2839–2864.
Fletcher, W.J., Müller, U.C., Koutsodendris, A., Christanis, K., Pross, J., 2013. A centennial-scale record of vegetation and climate variability from 312 to 240 ka (Marine Isotope Stages 9c–a, 8 and 7e) from Tenaghi Philippon, NE Greece. *Quaternary Science Reviews* 78, 108–125.
Ganopolski, A., Winkelmann, R., Schellnhuber, H.J., 2016. Critical insolation–CO_2 relation for diagnosing past and future glacial inception. *Nature* 529, 200–203.
Gibbard, P.L., 2013. Climatostratigraphy. In: *The Encyclopedia of Quaternary Science*. 2nd ed, Vol. 4. Elsevier, Amsterdam, the Netherlands, pp. 222–226.
Gibbard, P.L., West, R.G., 2000. Quaternary chronostratigraphy: the terminology of terrestrial sequences. *Boreas* 29, 329–336.
Gibbard, P.L., West, R.G., Boreham, S., Rolfe, C.J., 2011. Late Middle Pleistocene ice-marginal sedimentation in East Anglia, England. *Boreas* 41, 319–336.
Gibbard, P.L., West, R.G., Hughes, P.D., 2018. Pleistocene glaciation of Fenland, England, and its implications for evolution of the region. *Royal Society Open Science* 4, 170736. http://dx.doi.org/10.1098/rsos.170736.
Gillespie, A., Molnar, P., 1995. Asynchronous maximum advances of mountain and continental glaciers. *Reviews of Geophysics* 33, 311–364.
Giraudi, C., Bodrato, G., Ricci Lucchi, M., Cipriani, N., Villa, I.M., Giaccio, B., Zuppi, G.M., 2011. The Middle and late Pleistocene glaciations in the Campo Felice basin (Central Apennines, Italy). *Quaternary Research* 75, 219–230.
Giraudi, C., Giaccio, B., 2017. Middle Pleistocene glaciations in the Apennines, Italy: new chronological data and preservation of the glacial record. *Geological Society of London Special Publication* 433, 161–178.
Hao, Q., Wang, L., Oldfield, F., Guo, Z., 2015. Extra-long interglacial during MIS 15–13 arising from limited extent of Arctic ice sheets in glacial MIS 14. *Scientific Reports* 5, 12103.
Harzhauser, M., Daxner-Höck, G., López-Guerrero, P., Maridet, O., Oliver, A., Piller, W.E., Richoz, S., Erbajeva, M.A., Neubauer, T. A., Göhlich, U.B., 2016. Stepwise onset of the Icehouse world and its impact on Oilgo-Miocene Centra Asian mammals. *Scientific Reports* 6, 36169. doi: 10.1038/srep36169.
Hays, J.D., Imbrie, J., Shackleton, N.J., 1976. Variations in the Earth's orbit: pacemaker of the ice ages. *Science* 194, 1121–1132.
Head, M.J., Gibbard, P.L., 2005. Early–Middle Pleistocene transitions: an overview and recommendations for the defining boundary. *Geological Society of London Special Publication* 247, 1–18.
Head, M.J., Gibbard, P.L., 2015. Formal subdivision of the Quaternary system/period: past, present, and future. *Quaternary International* 383, 4–35.
Hodell, D.A., Channell, J.E.T., Curtis, J.H., Romero, O.E., Röhl, U., 2008. Onset of "Hudson Strait" Heinrich events in the Eastern North Atlantic at the end of the Middle Pleistocene Transition (~640 ka). *Paleoceanography* 23, PA4218.
Hönisch, B., Hemming, N.G., Archer, D., Siddall, M., McManus, J.F., 2009. Atmospheric carbon dioxide concentration across the mid-Pleistocene transition. *Science* 324, 1551–1554.
Hughes, P.D., 2008. Response of a Montenegro glacier to extreme summer heatwaves in 2003 and 2007. *Geografiska Annaler* 90A, 259–267.
Hughes, P.D., 2009. Twenty-first century glaciers in the Prokletije mountains, Albania. *Arctic, Antarctic and Alpine Research* 41, 455–459.
Hughes, P.D., Braithwaite, R.J., 2008. Application of a degree-day model to reconstruct Pleistocene glacial climates. *Quaternary Research* 69, 110–116.
Hughes, P.D., Gibbard, P.L., 2015. A stratigraphical basis for the Last Glacial Maximum (LGM). *Quaternary International* 383, 174–185.
Hughes, P.D., Gibbard, P.L., Ehlers, J., 2013. Timing of glaciation during the last glacial cycle: evaluating the meaning and significance of the "Last Glacial Maximum" (LGM). *Earth Science Reviews* 125, 171–198.
Hughes, P.D., Gibbard, P.L., Woodward, J.C., 2005. Quaternary glacial records in mountain regions: a formal stratigraphical approach. *Episodes* 28, 85–92.
Hughes, P.D., Woodward, J.C., Gibbard, P.L., Macklin, M.G., Gilmour, M.A., Smith, G.R., 2006. The glacial history of the Pindus Mountains, Greece. *Journal of Geology* 114, 413–434.
Hughes, P.D., Woodward, J.C., van Calsteren, P.C., Thomas, L.E., 2011. The glacial history of the Dinaric Alps, Montenegro. *Quaternary Science Reviews* 30, 3393–3412.
Hughes, P.D., Woodward, J.C., van Calsteren, P.C., Thomas, L.E., Adamson, K., 2010. Pleistocene ice caps on the coastal mountains of the Adriatic Sea: palaeoclimatic and wider palaeoenvironmental implications. *Quaternary Science Reviews* 29, 3690–3708.
Imbrie, J., Berger, A., Boyle, E.A., Clemens, S.C., Duffy, A., Howard, W.R., Kukla, G., et al., 1993. On the structure and origin of major glaciation cycles 2. The 100,000-year cycle. *Paleoceanography* 8, 699–735.
Imbrie, J., Hays, J.D., Martinson, D.G., McIntyre, A., Mix, A.C., Morley, J.J., Pisias, N.G., Prell, W.L., Shackleton, N.J., 1984. The orbital theory of Pleistocene climate: support from a revised chronology of the marine 18O record. In: Berger, A., Imbrie, J., Hays, G., Kukla, G., Saltzman, B. (Eds.), *Milankovitch and Climate*. Reidel, Dordrecht, Netherlands, pp. 269–306.
Jouzel, J., Masson-Delmotte, V., Cattani, O., Dreyfus, G., Falourd, S., Hoffmann, G., Minster, B., et al., 2007a. Orbital and millennial Antarctic climate variability over the last 800,000 years. *Science* 317, 793–796.
Jouzel, J., Stievenard, M., Johnsen, S.J., Landais, A., Masson-Delmotte, V., Sveinbjornsdottir, A., Vimeux, F., von Grafenstein, U., White, J.W.C., 2007b. The GRIP deuterium-excess record. *Quaternary Science Reviews* 26, 1–17.
Jouzel, J., Masson-Delmotte, V., Cattani, O., Dreyfus, G., Falourd, S., Hoffmann, G., Minster, B., et al., 2007c. *EPICA Dome C Ice Core 800KYr Deuterium Data and Temperature Estimates. IGBP PAGES/World Data Center for Paleoclimatology. Data Contribution Series #2007-091*. NOAA/NCDC Paleoclimatology Program, Boulder, CO. ftp://ftp.ncdc.noaa.gov/pub/data/paleo/icecore/antarctica/epica_domec/edc3deuttemp2007.txt (accessed May 4, 2018).
Joy, K., Fink, D., Storey, B., De Pascale, G.P., Quigley, M., Fujioka, T., 2017. Cosmogenic evidence for limited local LGM glacial expansion, Denton Hills, Antarctica. *Quaternary Science Reviews* 178, 89–101.
Kukla, G., An, Z. S., Melice, J. L., Gavin, J., Xiao, J. L., 1994. Magnetic susceptibility record of Chinese Loess. *Transactions of the Royal Society of Edinburgh, Earth Science* 81, 263–288.
Laban, C., van der Meer, J.M., 2011. Pleistocene glaciation in the Netherlands. In: Ehlers, J., Gibbard, P.L., Hughes, P.D. (Eds.), *Quaternary Glaciations—Extent and Chronology: A Closer Look*. Vol. 15, *Developments in Quaternary Science*. Elsevier, Amsterdam, pp. 247–260.

https://doi.org/10.1017/qua.2018.37 Published online by Cambridge University Press

Labeyrie, L.D., Duplessy, J.C., Blanc, P.L., 1987. Variations in mode of formation and temperature of oceanic deep waters over the past 125,000 years. *Nature* 327, 477–482.

Lamb, R.M., Huuse, M., Stewart, M., 2016. Early Quaternary sedimentary processes and palaeoenvironments in the central North Sea. *Journal of Quaternary Science* 32, 127–144.

Lambert, F., Bigler, M., Steffensen, J.P., Hutterli, M., Fischer, H., 2012. Centennial mineral dust variability in high-resolution ice core data from Dome C, Antarctica. *Climate of the Past* 8, 609–623.

Lambert, F., Delmonte, B., Petit, J.R., Bigler, M., Kaufmann, P.R., Hutterli, M.A., Stockler, T.F., Ruth, U., Steffensen, J.P., Maggi, V., 2008. Dust–climate couplings over the past 800,000 years from the EPICA Dome C ice core. *Nature* 452, 616–619.

Lang, N., Wolff, E.W., 2011. Interglacial and glacial variability from the last 800 ka in marine, ice and terrestrial archives. *Climate of the Past* 7, 361–380.

Larsen, E., Kjær, K.H., Demidov, I.N., Funder, S., Grøsfjeld, K., Houmark-Nielsen, M., Jensen, M., Linge, H., Lyså, A., 2006. Late Pleistocene glacial and lake history of northwestern Russia. *Boreas* 35, 394–424.

Laskar, J., Robutel, P., Joutel, F., Gastineau, M., Correia, A. C. M., Levrard, B., 2004. A long-term numerical solution for the insolation quantities of the Earth. *Astronomy and Astrophysics* 428, 261–285.

Lilly, K., Fink, D., Fabel, D., Lambeck, K., 2010. Pleistocene dynamics of the interior East Antarctic ice sheet. *Geology* 38, 703–706.

Lisiecki, L.E., Raymo, M.E., 2005. A Pliocene–Pleistocene stack of 57 globally distributed benthic $\delta^{18}O$ records. *Paleoceanography* 20, PA1003.

Lowe, J.J., Rasmussen, S.O., Björck, S., Hoek, W.Z., Steffensen, J.P., Walker, M.J.C., Yu, Z., INTIMATE Group, 2008. Synchronisation of palaeoenvironmental events in the North Atlantic region during the Last Termination: a revised protocol recommended by the INTIMATE Group. *Quaternary Science Reviews* 27, 6–17.

Lüthi, D., Floch, M. Le, Bereiter, B., Blunier, T., Barnola, J-M., Raynaud, D., Jouzel, J., Fischer, H., Kawamura, K., Stocker, T.F., 2008. High-resolution carbon dioxide concentration record 650,000–800,000 years before present. *Nature* 453, 379–381.

MacAyeal, D., 1993. Binge/purge oscillations of the Laurentide ice sheet as a cause of the North Atlantic's Heinrich events. *Paleoceanography* 8, 775–784.

Margari, V., Skinner, L.C., Hodell, D.A., Martrat, B., Toucanne, S., Grimalt, J.O., Gibbard, P.L., Lunkka, J.P., Tzedakis, P.C., 2014. Land-ocean changes on orbital and millennial time scales and the penultimate glaciation. *Geology* 42, 183–186.

Margari, V., Skinner, L.C., Tzedakis, P.C., Ganopolski, A., Vautravers, M., Shackleton, N.J., 2010. The nature of millennia-scale climate variability during the past two glacial periods. *Nature Geoscience* 3, 127–131.

Markle, B.R., Steig, E.J., Buizert, C., Schoenemann, S.W., Bitz, C. M., Fudge, T.J., Redro, J.B., et al., 2017. Global atmospheric teleconnections during Dansgaard-Oeschger events. *Nature Geoscience* 10, 36–40.

Marks, L., 2011. Quaternary glaciations in Poland. In: Ehlers, J., Gibbard, P.L., Hughes, P.D. (Eds.), *Quaternary Glaciations—Extent and Chronology: A Closer Look*. Vol. 15, *Developments in Quaternary Science*. Elsevier, Amsterdam, pp. 299–304.

Martinson, D.G., Pisias, N.G., Hays, J.D., Imbrie, J., Moore, T.C., Shackleton, N.J., 1987. Age dating and the orbital theory of the ice ages: development of a high resolution 0–300,000 year chronostratigraphy. *Quaternary Research* 27, 1–29.

McManus, J.F., Oppo, D.W., Cullen, J.L., 1999. A 0.5 million-year record of millennial-scale climate variability in the North Atlantic. *Science* 283, 971–975.

Meyer, V.D., Barr, I.D., 2017. Linking glacier extent and summer temperature in NE Russia—implications for precipitation during the global Last Glacial Maximum. *Palaeogeography, Palaeoclimatology, Palaeoecology* 470, 72–80.

Misawa, K., Kohno, M., Tomiyama, T., Noguchi, T., Nakamura, T., Nagao, K., Mikouchi, T., Nishiizumi, K., 2010. Two extraterrestrial dust horizons found in the Dome Fuji ice core, East Antarctica. *Earth and Planetary Science Letters* 289, 287–297.

Mudelsee, M., Schulz, M., 1997. The Mid-Pleistocene transition: onset of 100 ka cycle lags ice volume build-up by 280 ka. *Earth and Planetary Science Letters* 151, 117–123.

Muttoni, G., Carcano, C., Garzanti, E., Ghielmi, M., Piccin, A., Pini, R., Rogledi, S., Sciunnach, D., 2003. Onset of major Pleistocene glaciations in the Alps. *Geology* 31, 989–992.

Narcisi, B., Petit, J.R., Engrand, C., 2007. First discovery of meteoritic events in deep Antarctic (EPICA-Dome C) ice cores. *Geophysical Research Letters* 34, L15502.

National Oceanic and Atmospheric Administration, 2018. Antarctic Ice Cores Revised 800KYr CO_2 Data. http://ncdc.noaa.gov/paleo/study/17975 (accessed May 4, 2018).

Ohmura, A., Kasser, P., Funk, M., 1992. Climate at the equilibrium line of glaciers. *Journal of Glaciology* 38, 397–411.

Owen, L.A., Chen, J., Hedrick, K.A., Caffee, M.W., Robinson, A.C., Schoenbohm, M., Yuan, Z., Imrecke, D.B., Liu, J., 2012. Quaternary glaciation of the Tashgurkan Valley, southeast Pamir. *Quaternary Science Reviews* 47, 56–72.

Owen, L.A., Dortch, J.M., 2014. Nature and timing of Quaternary glaciation in the Himalaya–Tibetan orogeny. *Quaternary Science Reviews* 88, 14–54.

Owen, L.A., Robinson, R., Benn, D.I., Finkel, R.C., Davis, N.K., Yi, C., Putkonen, J., Li, D., Murray, A.S., 2009. Quaternary glaciation of Mount Everest. *Quaternary Science Reviews* 28, 1412–1433.

Owen, L.A., Yi, C., Finkel, R.C., Davis, N., 2010. Quaternary glaciation of Gurla Mandata (Naimon'anyi). *Quaternary Science Reviews* 29, 1817–1830.

Paillard, D., 2001. Glacial cycles: towards a new paradigm. *Reviews of Geophysics* 39, 325–346.

Pena, L.D., Goldstein, S.L., 2014. Thermohaline circulation crisis and impacts during the mid-Pleistocene transition. *Paleoceanography* 345, 318–322.

Rabassa, J., Coronato, A.M., Salemme, M., 2005. Chronology of the Last Cenozoic Patagonian glaciations and their correlation with biostratigraphic units of the Pampean region (Argentina). *Journal of South American Earth Sciences* 20, 81–103.

Rabineau, M., Berné, S., Olivet, J.-L., Aslanian, D., Guillocheau, F., Joseph, P., 2006. Paleo sea-levels reconsidered from direct observations of paleoshoreline position during glacial maxima (for the last 500,000 yr). *Earth and Planetary Science Letters* 252, 119–137.

Railsback, L.B., Gibbard, P.L., Head, M.J., Voarintsoa, N.R.G., Toucanne, S., 2015. An optimized scheme of lettered marine isotope substages for the last 1.0 million years, and the climatostratigraphic nature of isotope stages and substages. *Quaternary Science Reviews* 111, 94–106.

Railsback, L.B., Xiao, H., Liang, F., Akers, P.D., Brook, G.A., Dennis, W.M., Lanier, T.E., Tan, M., Cheng, H., Edwards, R.L.,

https://doi.org/10.1017/qua.2018.37 Published online by Cambridge University Press

2014. A stalagmite record of abrupt climate change and possible westerlies-derived atmospheric precipitation during the Penultimate Glacial Maximum in northern China. *Palaeogeography, Palaeoclimatology, Palaeoecology* 393, 30–44.

Raymo, M.E., 1997. The timing of major climate terminations. *Paleoceanography and Paleoclimatology* 12, 577–585.

Regattieri, E., Zanchetta, G., Drysdale, R.N., Isola, I., Hellstrom, J.C., Roncioni, A., 2014. A continuous stable isotope record from the penultimate glacial maximum to the Last Interglacial (159–121 ka) from Tana Che Urla Cave (Apuan Alps, central Italy). *Quaternary Research* 82, 450–461.

Rial, J.A., 1999. Pacemaking the ice ages by frequency modulation of Earth's orbital eccentricity. *Science* 285, 564–568.

Ridgwell., A., Watson, A.J., Raymo, M.E., 1999. Is the spectral signature of the 100 kyr glacial cycle consistent with a Milankovitch origin? *Paleoceanography* 14, 437–440.

Rodrigues, T., Voelker, A.H.L., Grimalt, J.O., Abrantes, F., Naughton, F., 2011. Iberian Margin sea surface temperature during MIS 15 to 9 (380–300 ka): glacial suborbital variability versus interglacial stability. *Paleoceanography* 26, PA1204.

Rohling, E.J., Hibbert, F.D., Williams, F.H., Grant, K.M., Marino, G., Foster, G.L., Hennekam, R., et al., 2017. Differences between the last two glacial maxima and implications for ice-sheet? ^{18}O, and sea-level reconstructions. *Quaternary Science Reviews* 176, 1–28.

Roskosch, J., Winsermann, J., Polom, U., Brandes, C., Tsukamoto, S., Weitkamp, A., Batholomäus, W.A., Henningsen, D., Frechen, M., 2014. Luminescence dating of ice-marginal deposits in northern Germany: evidence for repeated glaciations during the Middle Pleistocene (MIS 12 to MIS 6). *Boreas* 44, 103–126.

Roucoux, K.H., Tzedakis, P.C., Lawson, I.T., Margari, V., 2011. Vegetation history of the penultimate glacial period (Marine Isotope Stage 6) at Ioannina, north-west Greece. *Journal of Quaternary Science* 26, 616–626.

Ruddiman, W.F., Raymo, M.E., Martinson, D.G., Clement, B.M., Backman, J., 1989. Pleistocene evolution of Northern Hemisphere climate. *Paleoceanography* 4, 353–412.

Seong, Y.B., Owen, L.A., Bishop, M.P., Bush, A., Clendon, P., Copland, P., Finkel, R.C., Kamp, U., Shroder, J.F., 2007. Quaternary glacial history of the Central Karakoram. *Quaternary Science Reviews* 26, 3384–3405.

Seong, Y.B., Owen, L.A., Yi, C., Finkel, R.C., Schoenbohm, L., 2009. Geomorphology of anomalously high glaciated mountains at the northwestern end of Tibet: Muztag Ata and Kongur Shan. *Geomorphology* 103, 227–250.

Shackleton, N.J., 1967. Oxygen isotope analyses and Pleistocene temperatures re-assessed. *Nature* 215, 15–17.

Shackleton, N.J., 1987. Oxygen isotopes, ice volume and sea level. *Quaternary Science Reviews* 6, 183–190.

Shackleton, N.J., 2000. The 100,000-year ice-age cycle identified and found to lag temperature, carbon dioxide, and orbital eccentricity. *Science* 289, 1897–1902.

Shackleton, N.J., Chapman, M., Sánchez-Goñi, M.F., Pailler, D., Lancelot, Y., 2002. The classic marine isotope substage 5e. *Quaternary Research* 58, 14–16.

Shackleton, N.J., Hall, M.A., Vincent, E., 2000. Phase relationships between millennial scale events 64,000–24,000 years ago. *Paleoceanography* 15, 565–569.

Shackleton, N.J., Sánchez-Goñi, M.F., Pailler, D., Lancelot, Y., 2003. Marine Isotope Substage 5e and the Eemain Interglacial. *Global and Planetary Change* 36, 151–155.

Shakun, J.D, 2017. Modest global-scale cooling despite extensive early Pleistocene ice sheets. *Quaternary Science Reviews* 165, 25–30.

Shakun, J. D., Lea, D.W., Lisiecki, L.E., Raymo, M.E., 2015. An 800-kyr record of global surface ocean δ^{18}O and implications for ice volume-temperature coupling. *Earth and Planetary Science Letters* 426, 58–68.

Scher, H.D., Martin, E.E., 2006. Timing and climatic consequences of the opening of the Drake Passage. *Science* 312, 428–430.

Skinner, L.C., Shackleton, N.J., 2005. An Atlantic lead over Pacific deep-water change across termination I: implications for the application of the marine isotope stage stratigraphy. *Quaternary Science Reviews* 24, 571–580.

Stenni, B., Buiron, D., Frezzoti, M., Albani, S., Barbante, C., Bard, E., Barnola, J. M., et al., 2011. Expression of the bipolar see-saw in Antarctic climate records during the last deglaciation. *Nature Geoscience* 4, 46–49.

Stirling, C.H., Esat, T.M., Lambeck, K., McCulloch, M.T., 1998. Timing and duration of the Last Interglacial: evidence for a restricted interval of widespread coral reef growth. *Earth and Planetary Science Letters* 160, 745–762.

Stocker, T. F., Johnsen, S. J., 2003. A minimum thermodynamic model for the bipolar seesaw. *Paleoceanography* 18, 1087.

Subcommission on Quaternary Stratigraphy, 2017. Regional Divisions (accessed February 27, 2018). https://quaternary.stratigraphy.org/regionaldivisions.

Svendsen, J.I., Alexanderson, H., Astakhov, V.I., Demidov, I., Dowdeswell, J.A., Funder, , S., Gataullin, V., et al., 2004. Late Quaternary ice sheet history of northern Eurasia. *Quaternary Science Reviews* 23, 1229–1271.

Syverson, K.M., Colgan, P.M., 2011. The Quaternary of Wisconsin: an updated review of stratigraphy, glacial history and landforms. In: Ehlers, J., Gibbard, P.L., Hughes, P.D. (Eds.), *Quaternary Glaciations—Extent and Chronology: A Closer Look*. Vol. 15, *Developments in Quaternary Science*. Elsevier, Amsterdam, pp. 537–552.

Toucanne, S., Zaragosi, S., Bourillet, J.F., Cremer, M., Eynaud, F., Van Vliet-Lanoë, B., Penaud, A., et al., 2009. Timing of massive "Fleuve manche" discharges over the last 350 kyr: insights into the European ice-sheet oscillations and the European drainage network from MIS 10 to 2. *Quaternary Science Reviews* 28, 1238–1256.

Tzedakis, P.C., Crucifix, M., Mitsui, T., Wolff, E.W., 2017. A simple rule to determine which insolation cycles lead to interglacials. *Nature* 542, 427–432.

Van Andel, T.H., 2002. The climate and landscape of the middle part of the Weichselian Glaciation in Europe: the Stage 3 project. *Quaternary Research* 57, 2–8.

Van Ginneken, M., Folco, L., Perchiazzi, N., Rochette, P., Bland, P.A., 2010. Meteoritic ablation debris from the Transantarctic Mountains: evidence for a Tunguska-like impact over Antarctica ca. 480 ka ago. *Earth and Planetary Science Letters* 293, 104–113.

Velichko, A.A., Faustova, M.A., Gribchenko, Y.N., Pisareva, V.V., Sudakova, N.G., 2004. Glaciations of the East European Plain—distribution and chronology. In: Ehlers, J., Gibbard, P.L. (Eds.), *Quaternary Glaciations—Extent and Chronology*. Part 1, *Europe*. Elsevier, Amsterdam, pp. 337–354.

Vorren, T.O., Landvik, J.Y., Andreassen, K., Laberg, J.S., 2011. Glacial history of the Barents Sea region. In: Ehlers, J., Gibbard, P.L., Hughes, P.D. (Eds.), *Quaternary Glaciations—Extent and Chronology: A Closer Look*. Vol. 15, *Developments in Quaternary Science*. Elsevier, Amsterdam, pp. 362–372.

Waelbroeck, C., Labeyrie, L., Michel, E., Duplessy, J.C., McManus, J.F., Lambeck, K., Balbon, E., Labracherie, M., 2002. Sea-level and deep

https://doi.org/10.1017/qua.2018.37 Published online by Cambridge University Press

water temperature changes derived from benthic foraminifera isotopic records. *Quaternary Science Reviews* 21, 295–305.

Walker, M.J.C., Johnsen, S., Rasmussen, S.O., Popp, T., Steffensen, J.-P., Gibbard, P.L, Hoek, W., et al., 2009. Formal definition and dating of the GSSP (Global Stratotype Section and Point) for the base of the Holocene using the Greenland NGRIP ice core, and selected auxiliary records. *Journal of Quaternary Science* 24, 3–17.

White, T.S., Bridgland, D.R., Westaway, R., Straw, A., 2017. Evidence for a late Middle Pleistocene glaciation of the British margin of the southern North Sea. *Journal of Quaternary Science* 32, 261–275.

Zhou, S.Z., Wang, X.L., Wang, J., Xu, L.B., 2006. A preliminary study on timing of the oldest Pleistocene glaciation in Qinghai–Tibetan Plateau. *Quaternary International* 154–155, 44–51.

https://doi.org/10.1017/qua.2018.37 Published online by Cambridge University Press